Supporting Information

Seven Coordinate Co(II) and Six Coordinate Ni(II) Complexes of Aromatic Macrocyclic Triamide Ligand as ParaCEST Agents for MRI

Rabindra N. Pradhan,[a] Subhayan Chakraborty,[b] Pratibha Bharti,[c] Janesh Kumar,[c] Arindam Ghosh,*[b] and Akhilesh K. Singh*[a]

[a]School of Basic Sciences, Indian Institute of Technology Bhubaneswar, Bhubaneswar, 752050 (India), E-mail: aksingh@iitbbs.ac.in
[b]School of Chemical Sciences, National Institute of Science Education and Research Bhubaneswar, 752050 (India), E-mail: aringh@niser.ac.in
[c]National Centre for Cell Science, NCCS Complex, Pune University Campus, Ganeshkhind, Pune- 411 007 (India)

NMR Spectra of the compounds

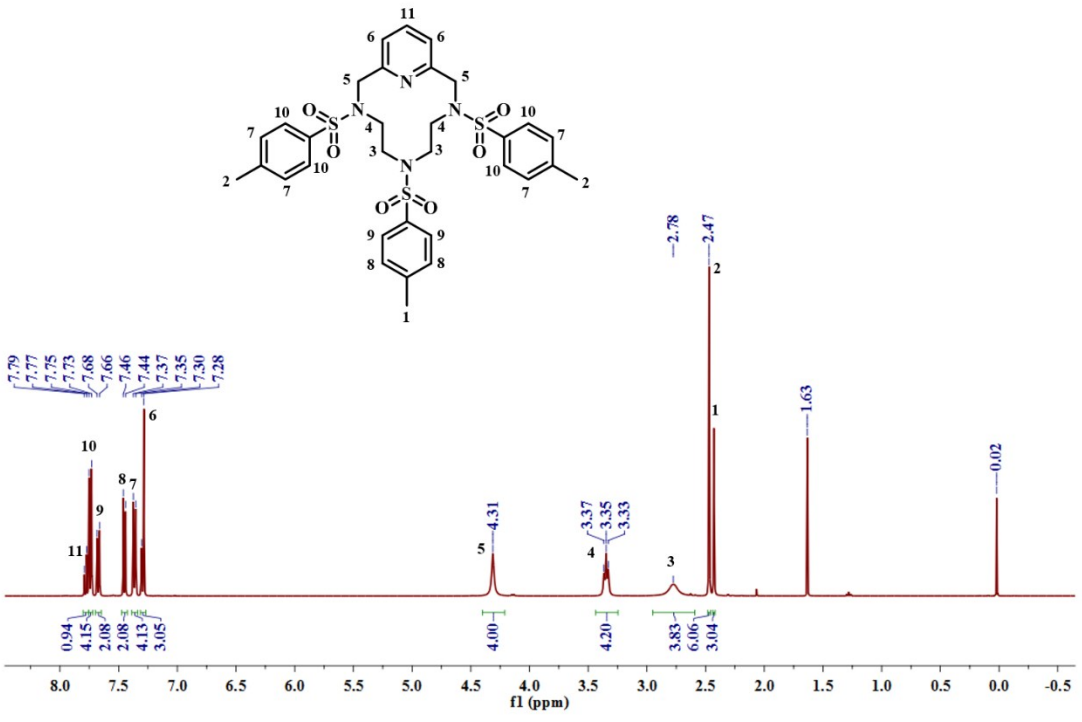

Fig. S1 ^{1}H NMR spectrum of compound **2** in $CDCl_3$

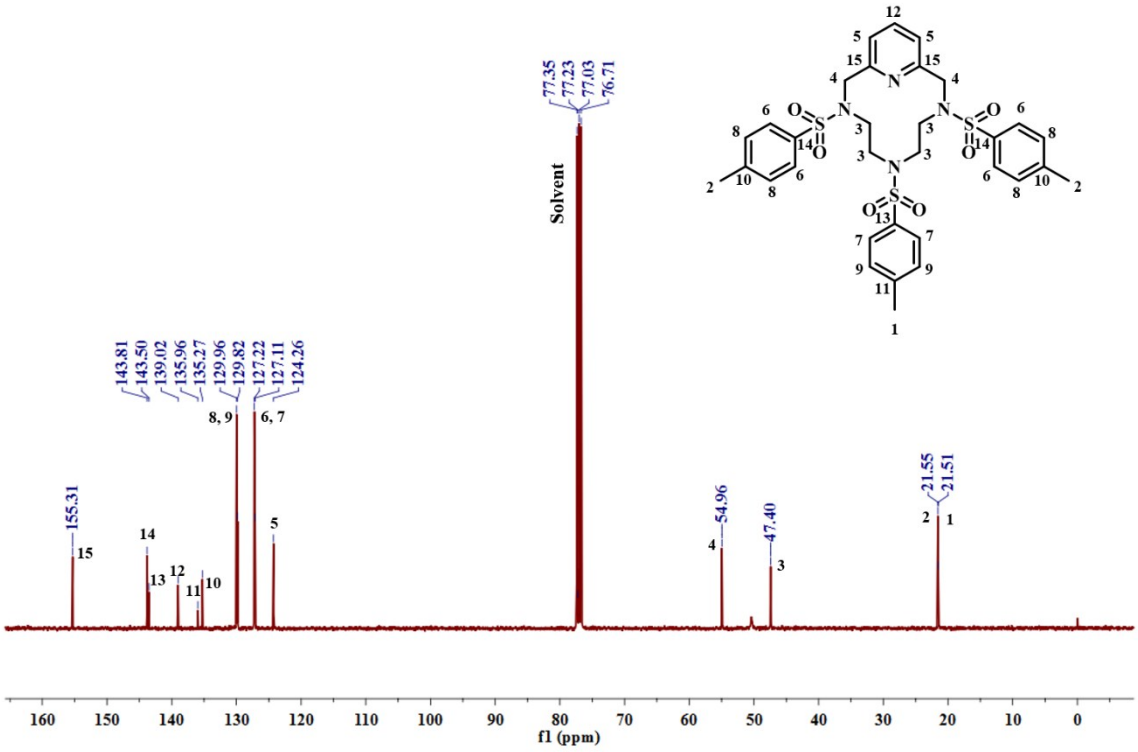

Fig. S2 ^{13}C NMR spectrum of compound **2** in $CDCl_3$

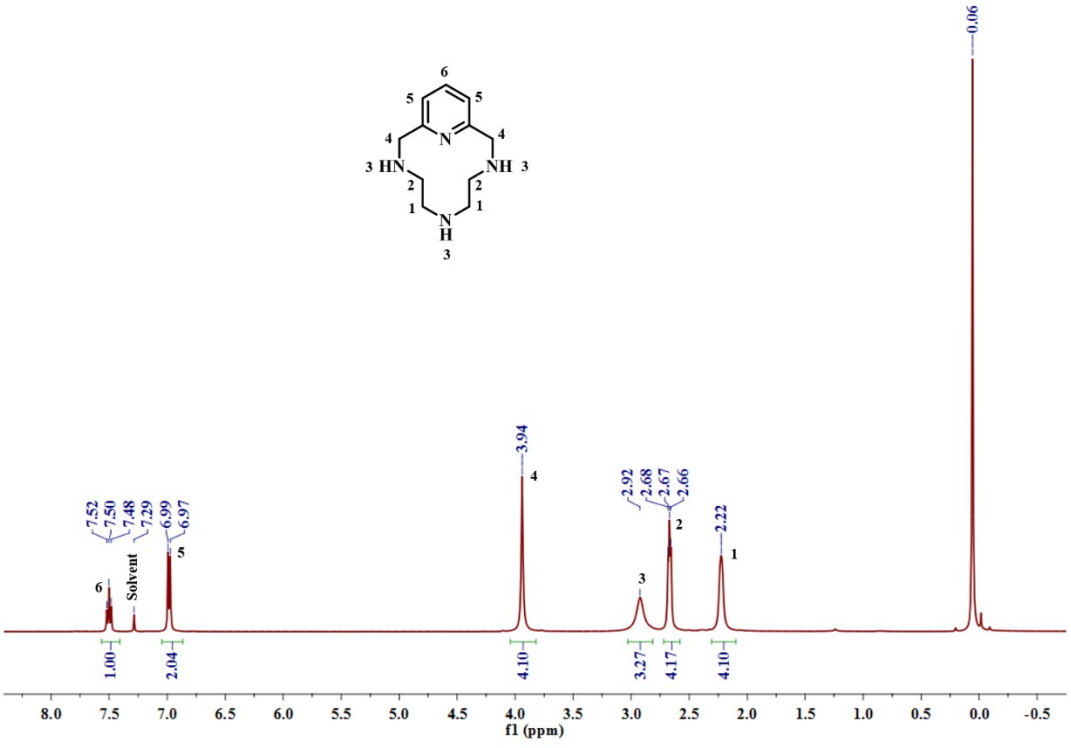

Fig. S3 ^{1}H NMR spectrum of compound **3** in $CDCl_3$

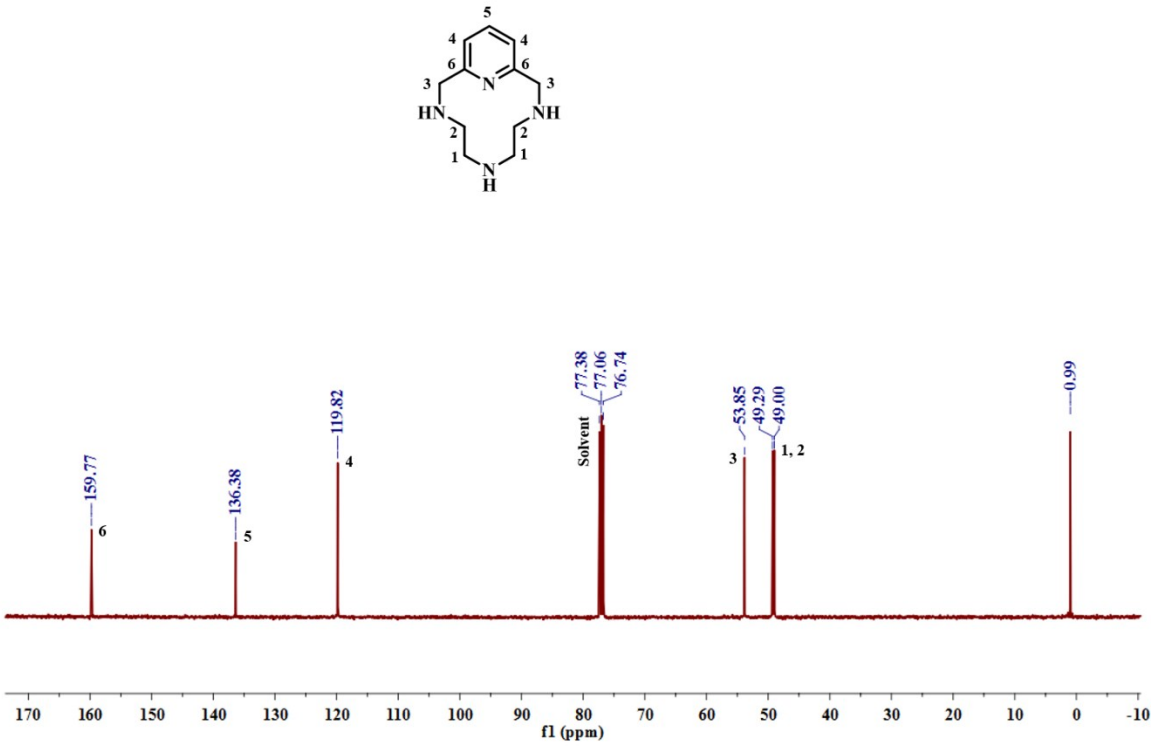

Fig. S4 ^{13}C NMR spectrum of compound **3** in $CDCl_3$

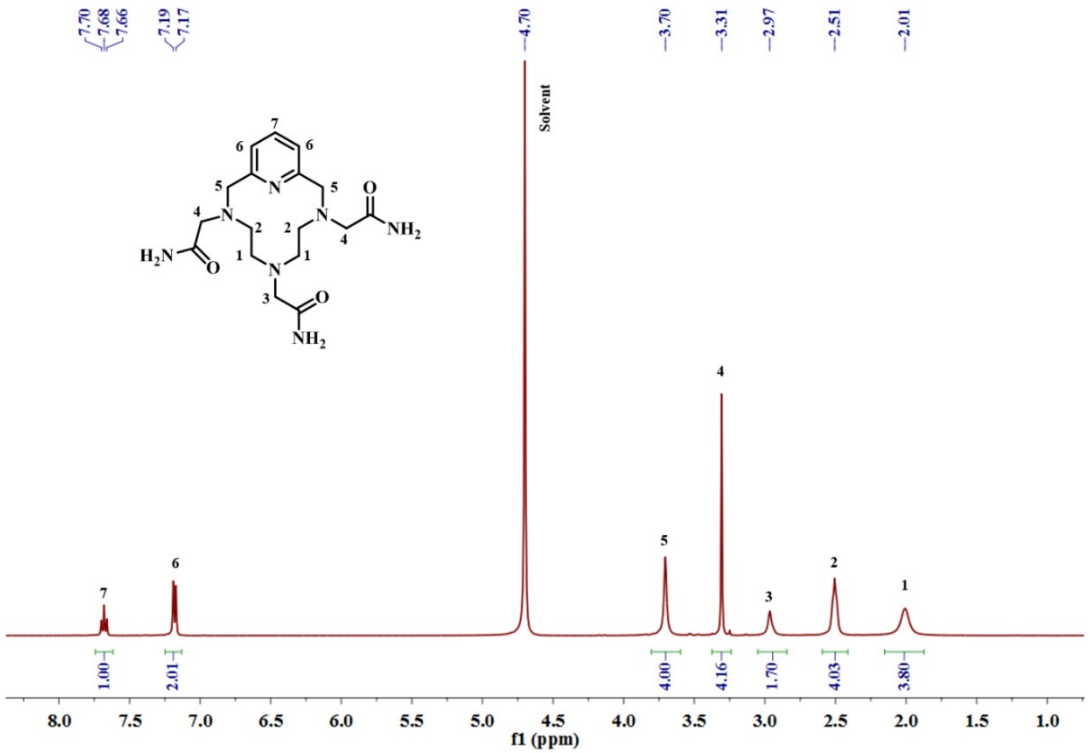

Fig. S5 ^{1}H NMR spectrum of ligand **TPTA** in D_2O.

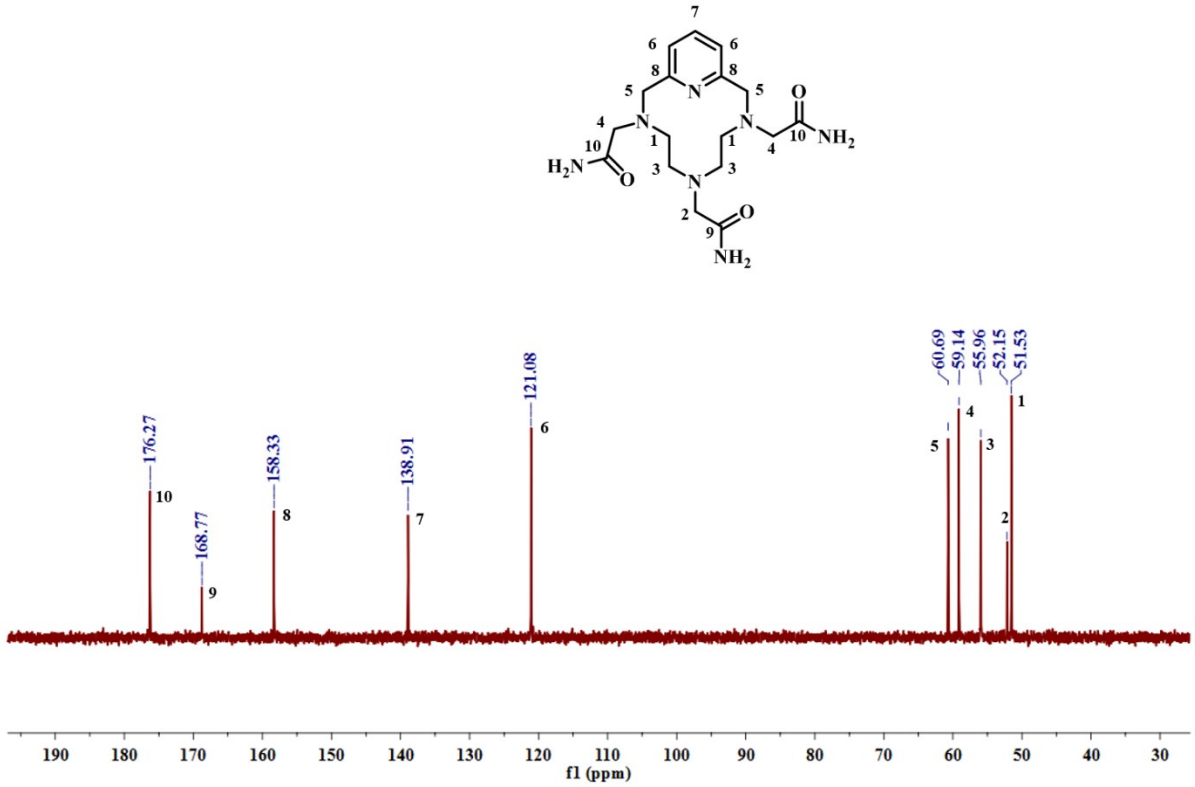

Fig. S6 ^{13}C NMR spectrum of ligand **TPTA** in D_2O.

ESI-MS spectra of compounds

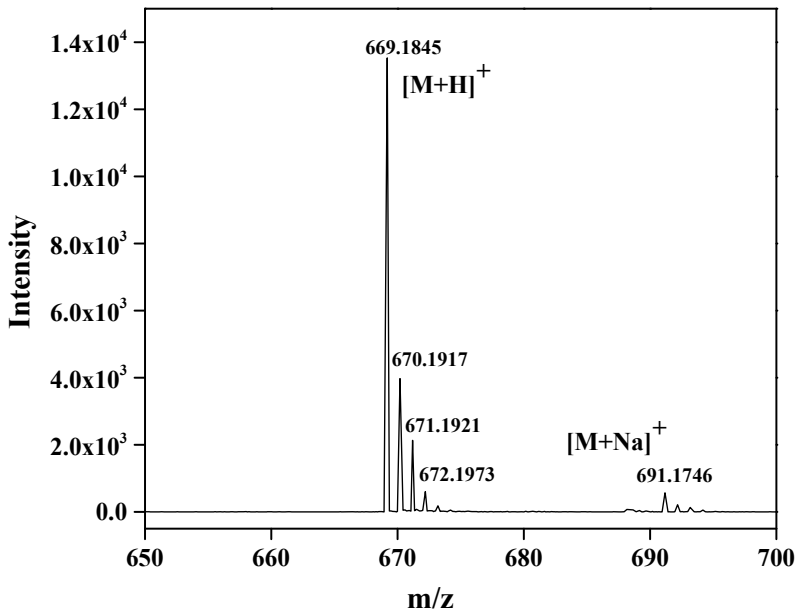

Fig. S7 ESI-MS spectrum of compound **2**.

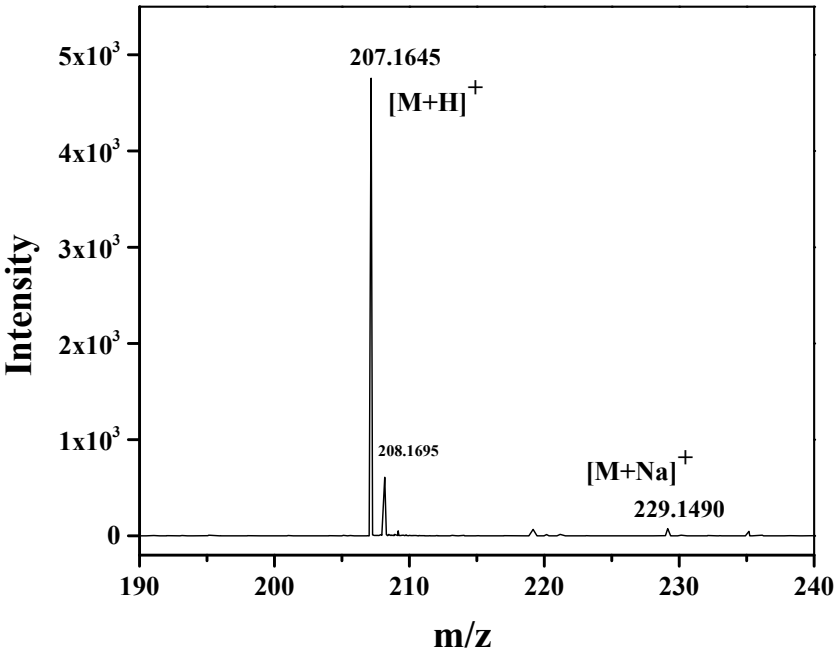

Fig. S8 ESI-MS spectrum of compound **3**.

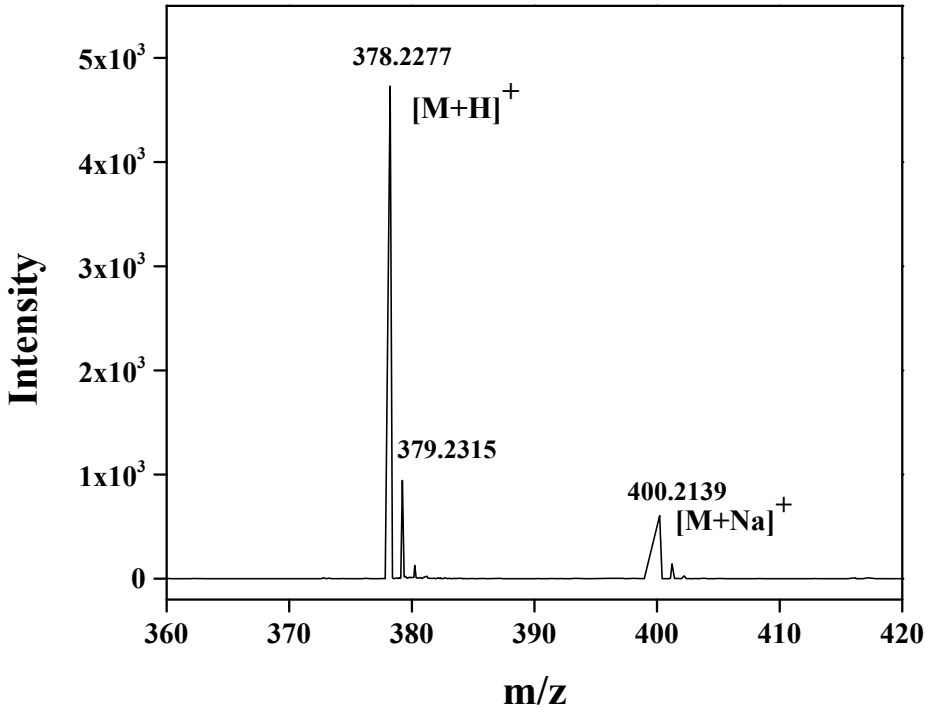

Fig. S9 ESI-MS spectrum of compound **TPTA**.

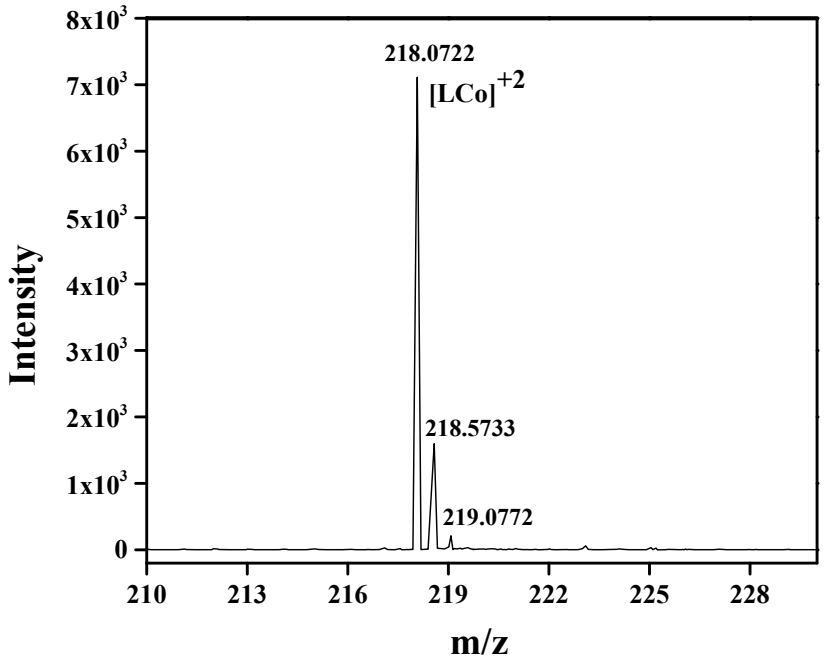

Fig. S10 ESI-MS spectrum of complex [Co(**TPTA**)]·Cl_2·$2H_2O$.

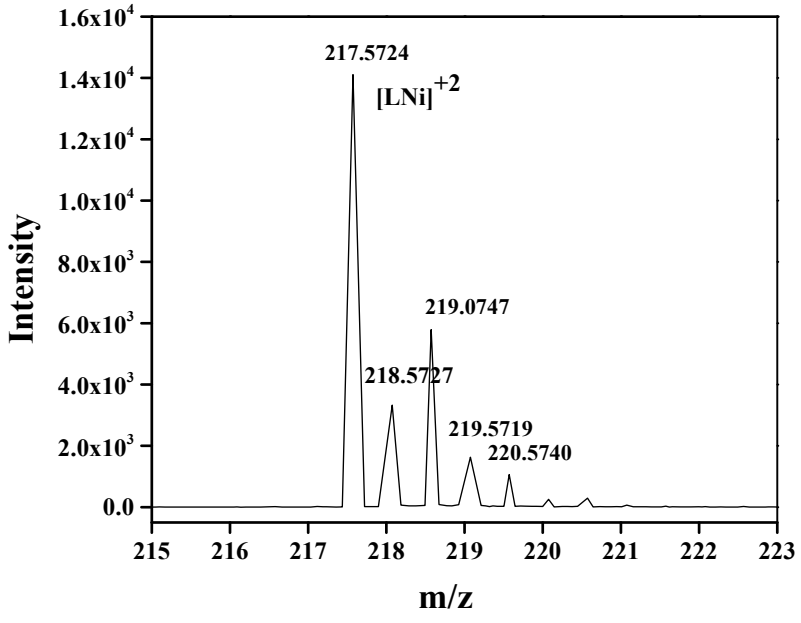

Fig. S11 ESI-MS spectrum of complex [Ni(**TPTA**)Cl]·Cl·$0.25H_2O$.

IR spectra of ligand and Complexes

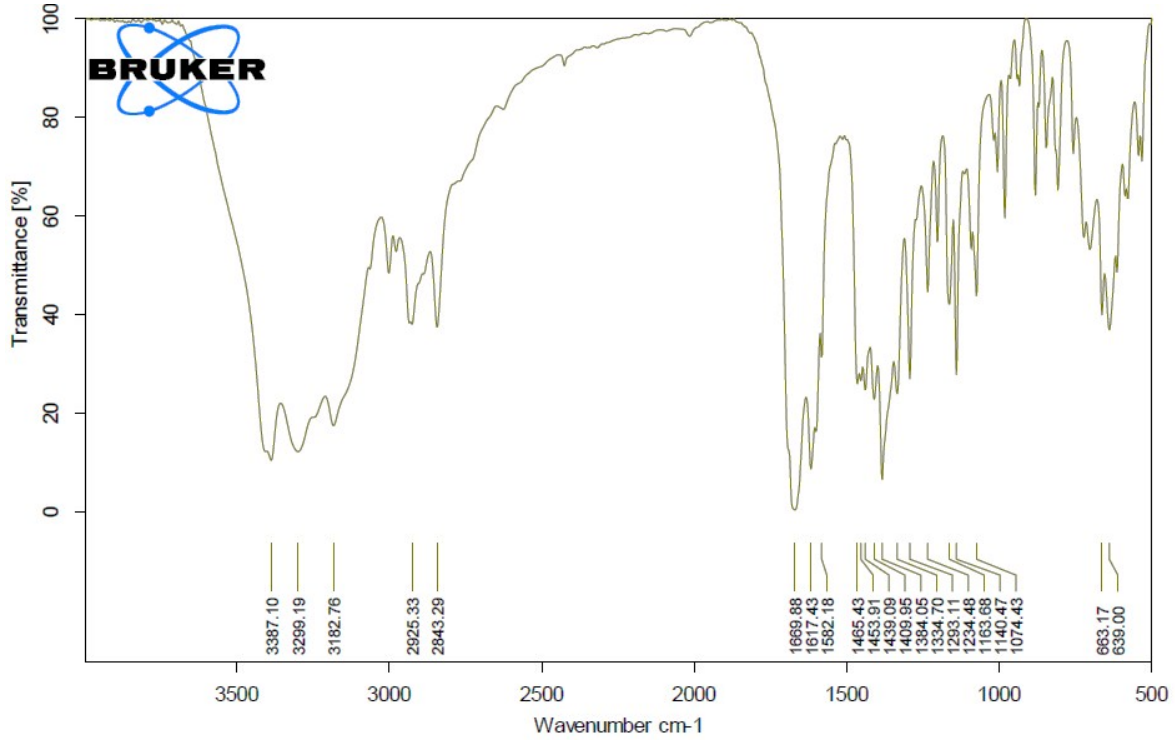

Fig. S12 FT-IR spectra of **TPTA** at ambient temperature.

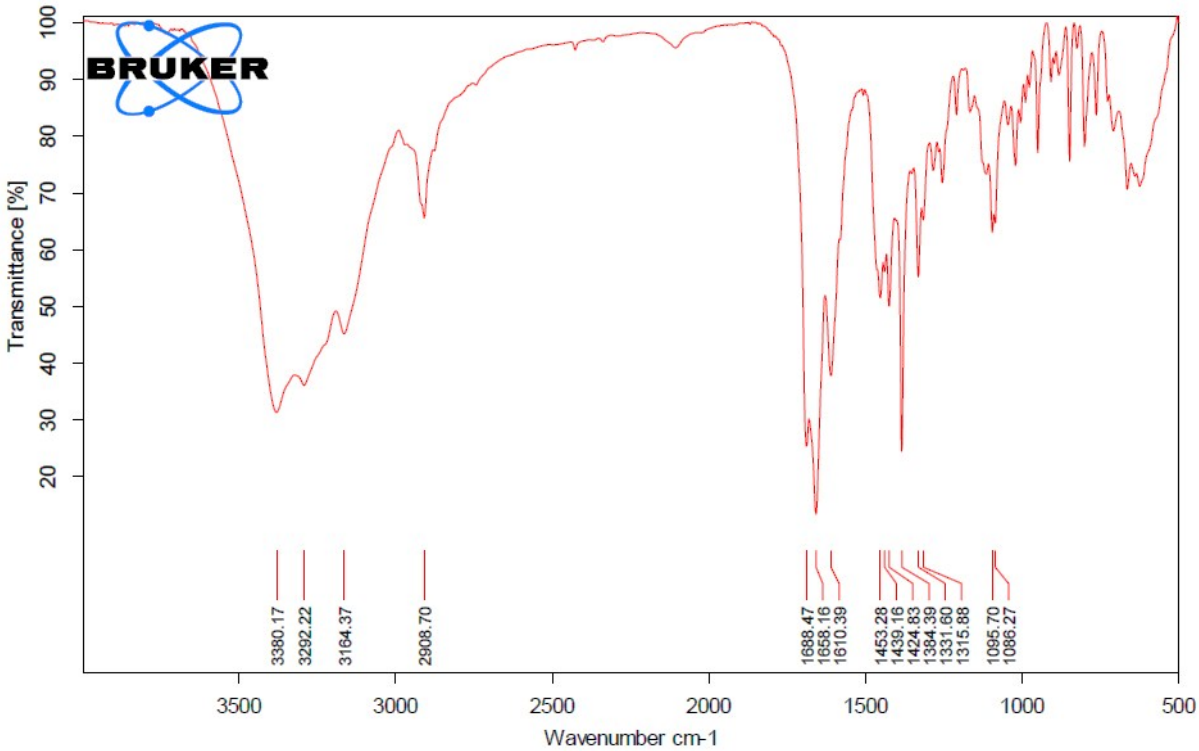

Fig. S13 FT-IR spectra of [Co(**TPTA**)]$^{+2}$ at ambient temperature.

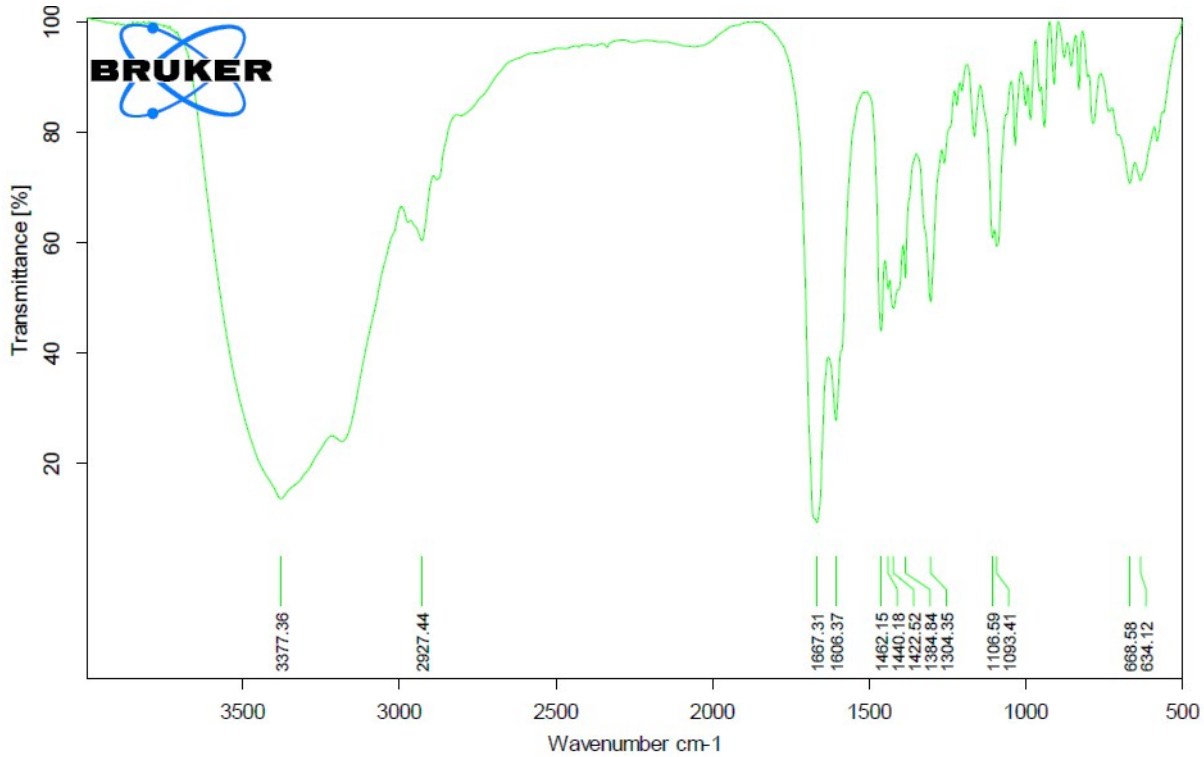

Fig. S14 FT-IR spectra of [Ni(**TPTA**)Cl]$^{+1}$ at ambient temperature.

UV-vis spectra of Complexes

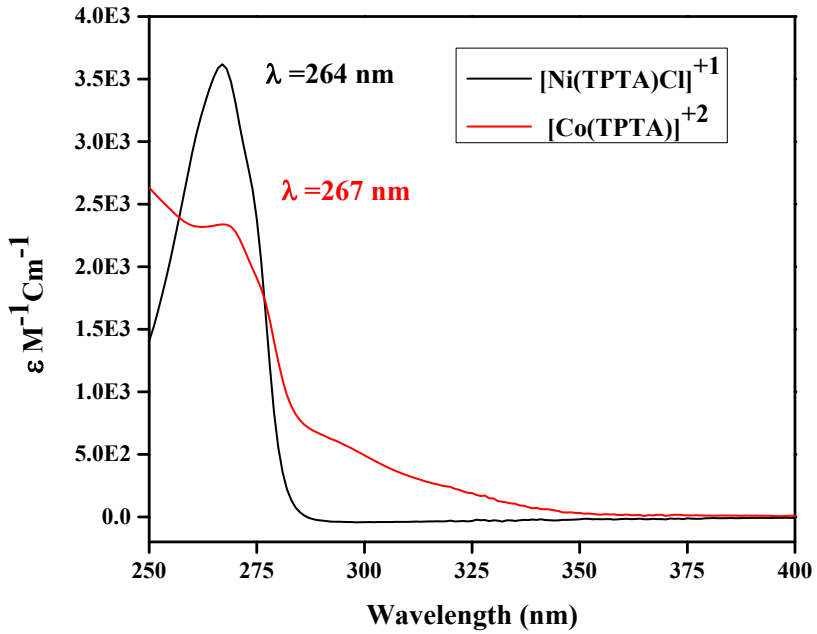

Fig. 15 UV-visible absorption spectra of 250 µM of [Co(**TPTA**)]$^{+2}$ (red) and [Ni(**TPTA**)Cl]$^{+1}$ in aqueous solutions containing 20 mM HEPES and 100 mM NaCl at ambient temperature.

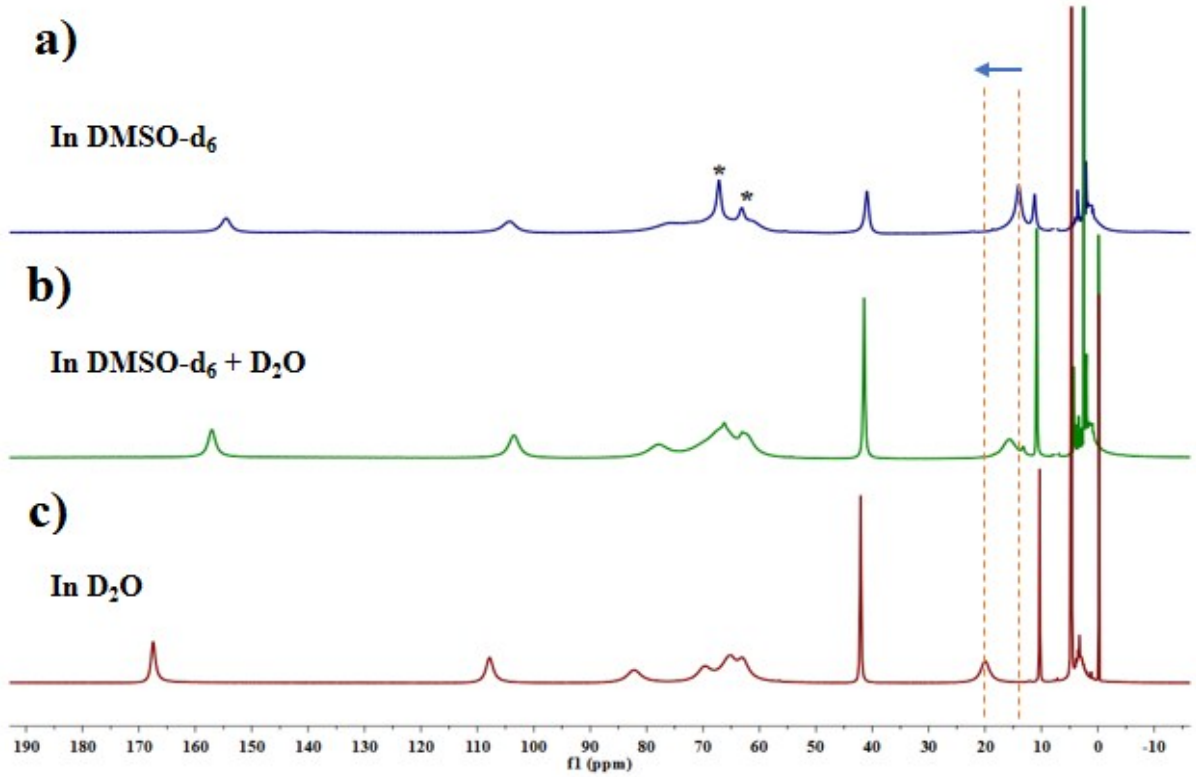

Fig. S16 ^{1}H NMR spectra of (a) [Co(**TPTA**)]$^{+2}$ in DMSO-d_6 (b) upon addition of 50 µL D_2O (c) [Co(**TPTA**)]$^{+2}$ in D_2O at ambient temperature. The exchangeable amide (NH) protons marked an asterisk (*).

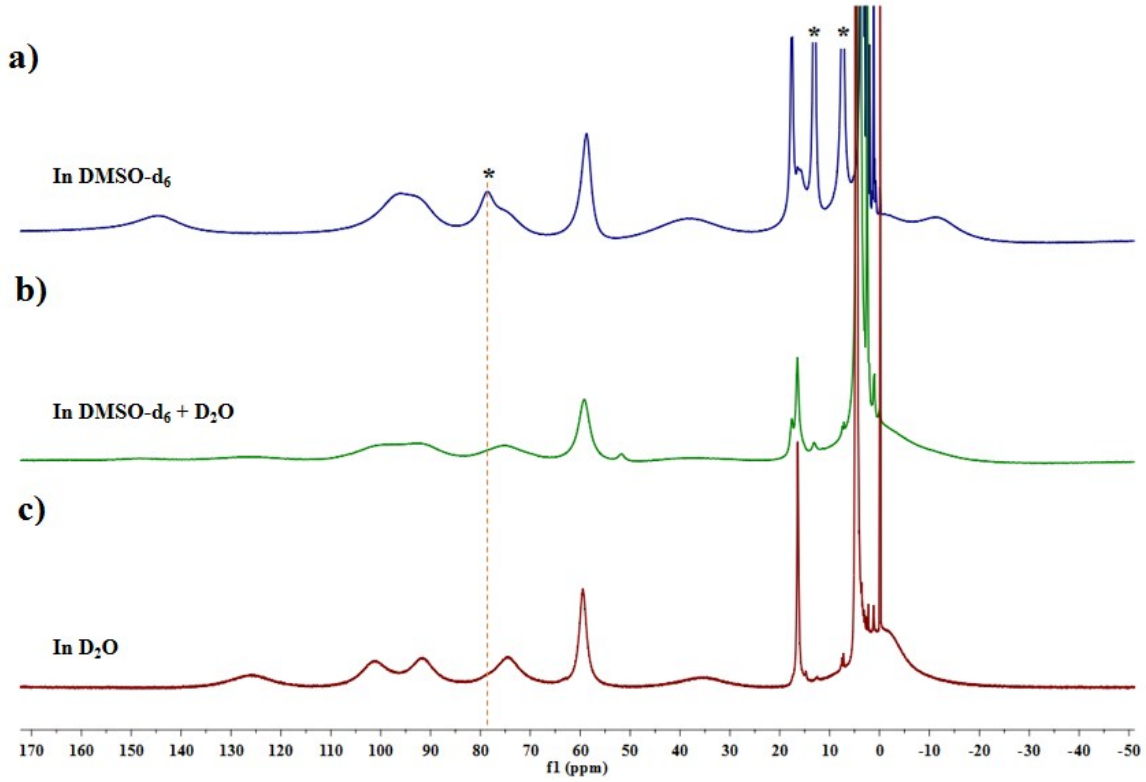

Fig. S17 ^{1}H NMR spectra of (a) [Ni(**TPTA**)Cl]$^{+1}$ in DMSO-d_6 (b) upon addition of 100 µL D_2O (c) [Ni(**TPTA**)Cl]$^{+1}$ in D_2O at ambient temperature. The exchangeable amide (NH) protons marked an asterisk (*).

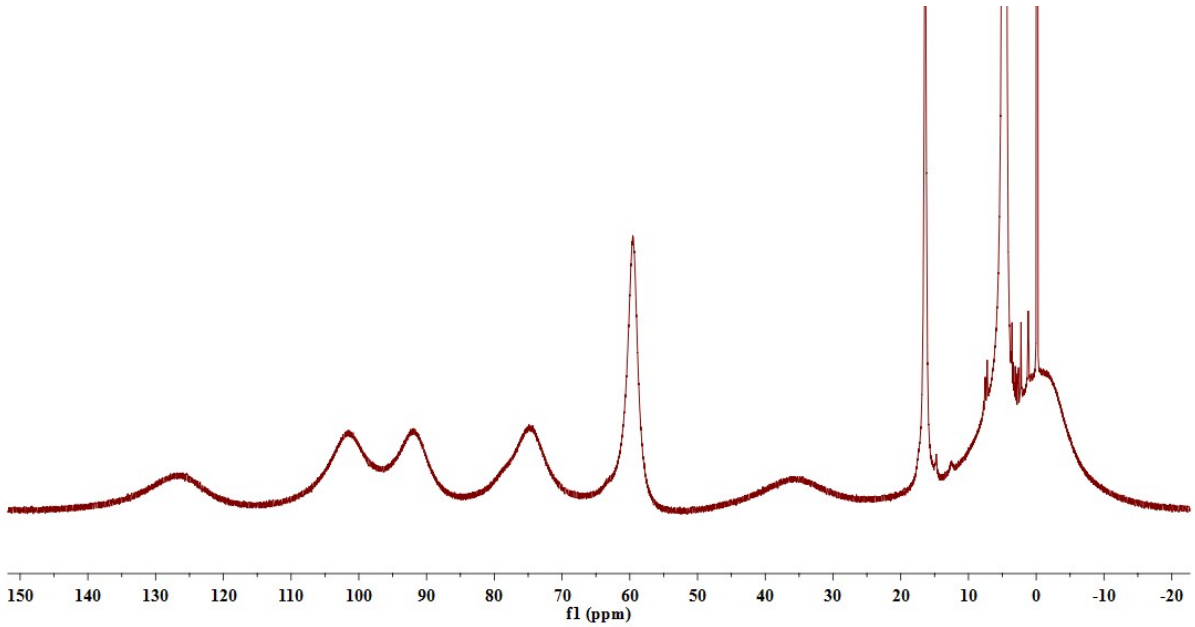

Fig. S18 ^{1}H NMR spectra of [Ni(**TPTA**)Cl]$^{+1}$ in D_2O.

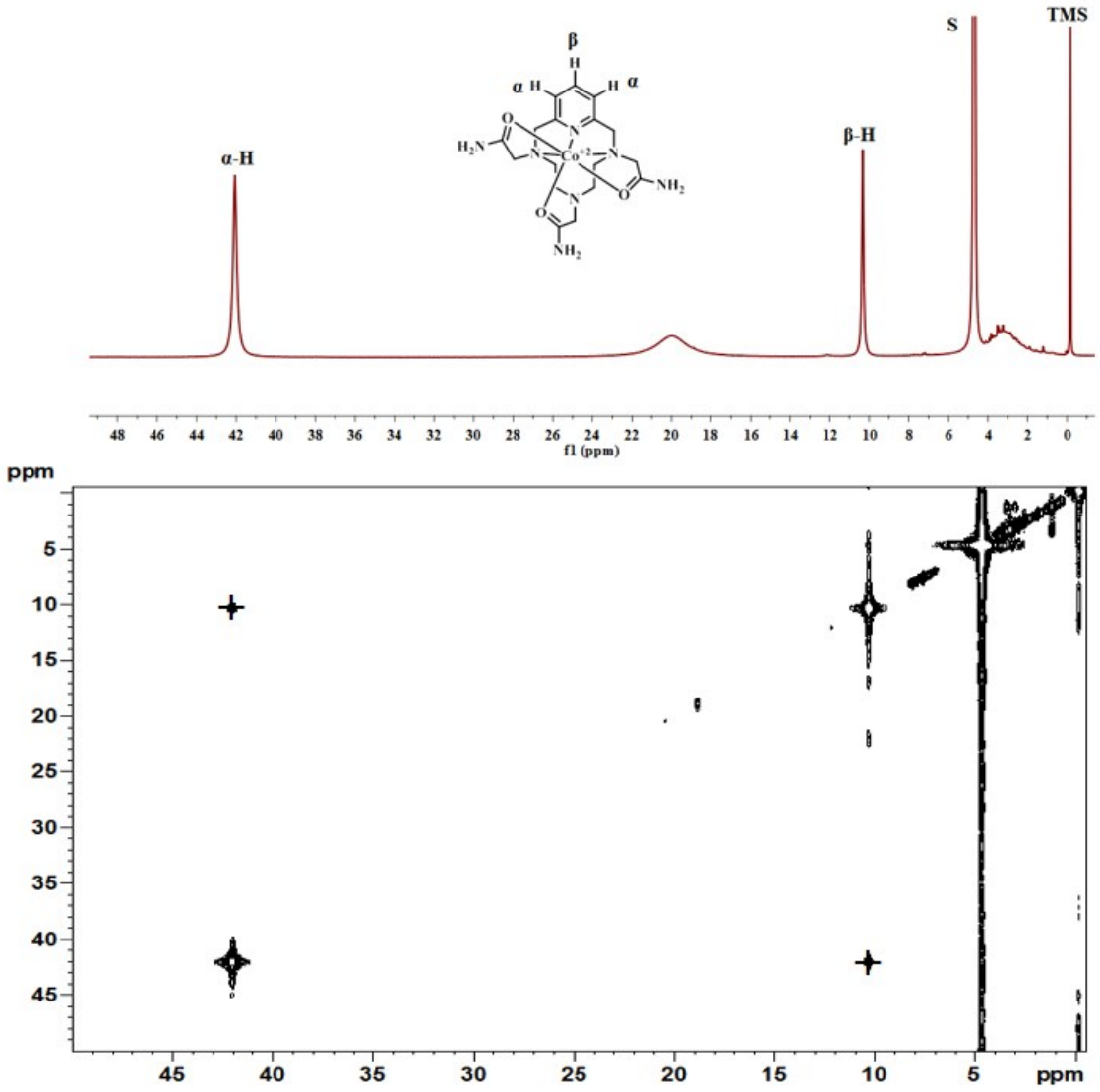

Fig. S19 Two-dimensional ^{1}H-^{1}H-COSY NMR spectrum (25 °C) obtained at 128 scans of 150 mM [Co(**TPTA**)]$^{+2}$ in D_2O (pD 7.0) showing the cross-peaks that allowed the identification of the proton resonances produced by aromatic protons of pyridine ring of the macrocyclic backbone.

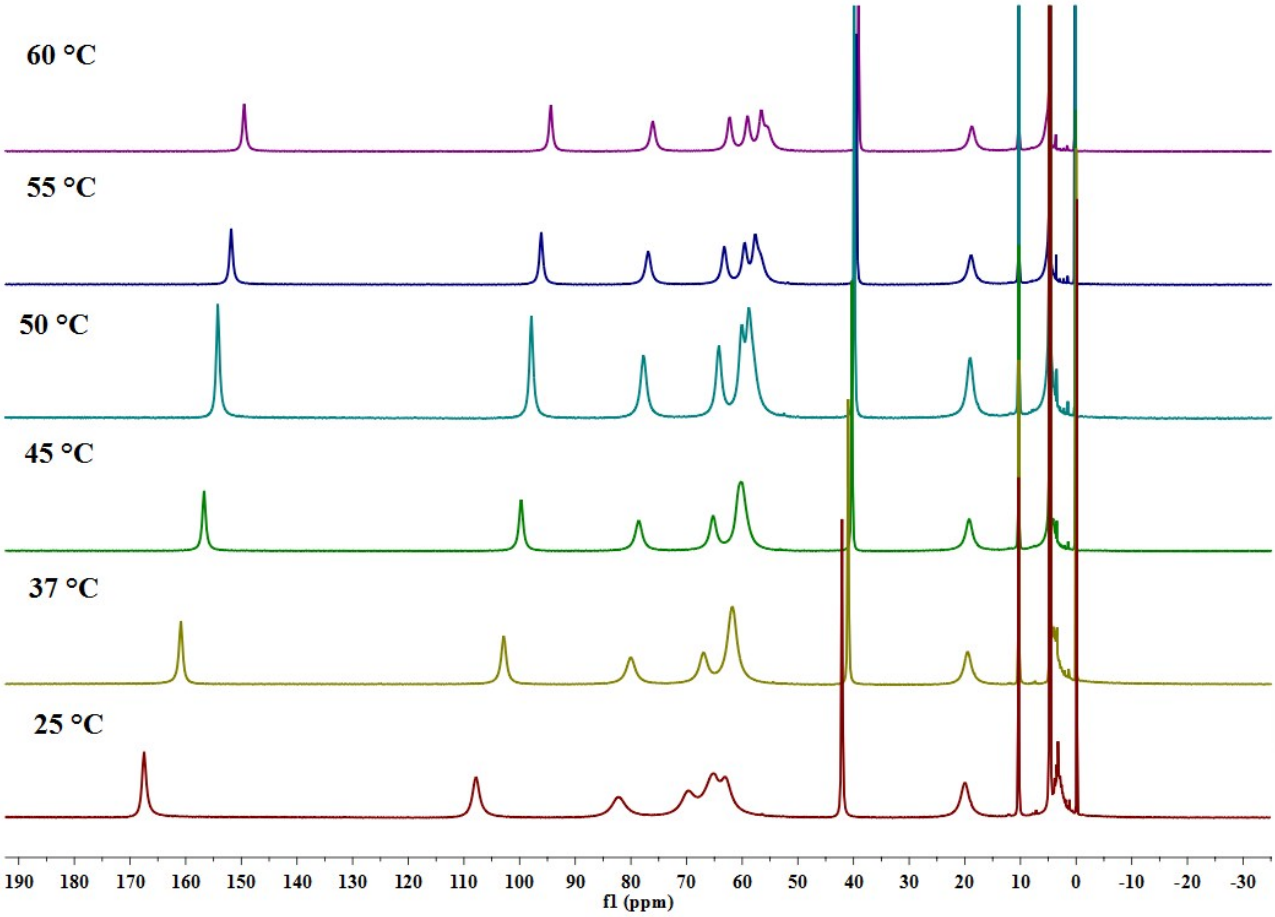

Fig. S20 ^{1}H NMR spectra of [Co(**TPTA**)]$^{+2}$ at varying temperature in D_2O from 25 °C to 60 °C.

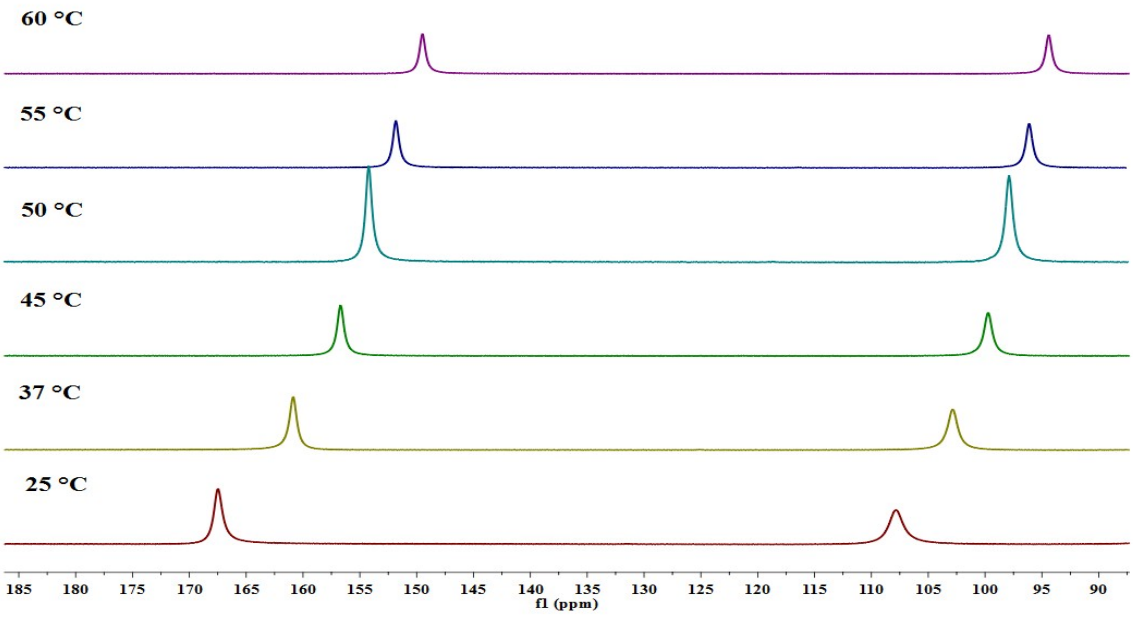

Fig. S21 Expansion showing ^{1}H NMR resonances of two downfield highly-shifted CH_2 peaks of [Co(**TPTA**)]$^{+2}$ at 25 to 60 °C in D_2O.

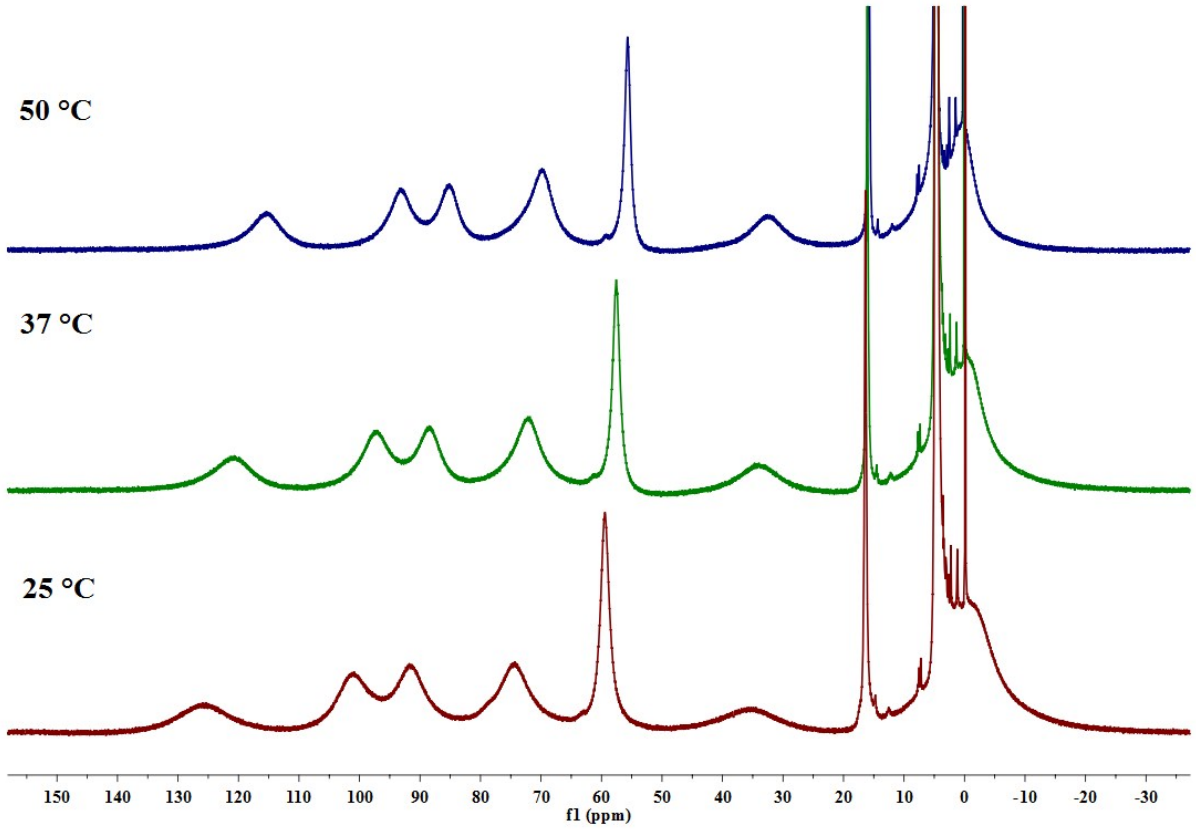

Fig. S22 ^{1}H NMR spectra of [Co(**TPTA**)]$^{+2}$ at varying temperature in D_2O from 25 °C to 50 °C.

Magnetic susceptibility measurement

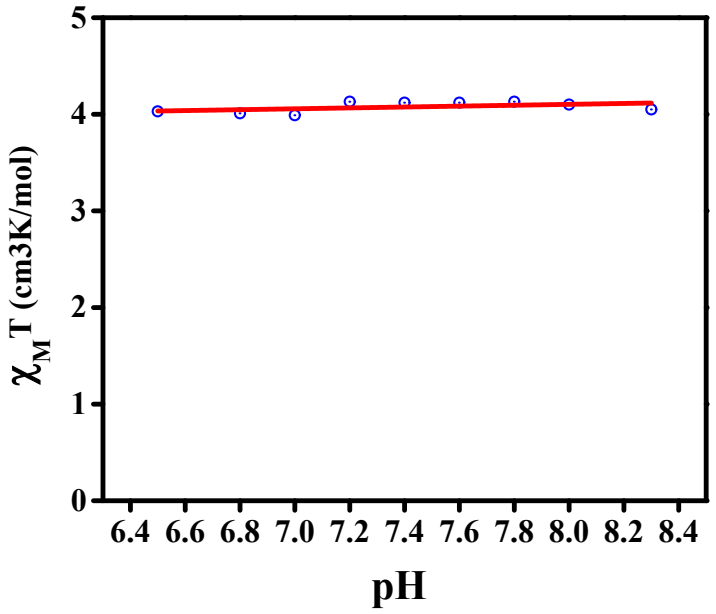

Fig. S23 Variable-pH magnetic susceptibility data for [Co(**TPTA**)]$^{+2}$ in aqueous solutions containing 20 mM HEPES and 100 mM NaCl at 37 °C, obtained using the Evans .Circles

represent experimental data and the solid black line denotes the average value of $\chi_M T = 4.07 \pm 0.1$ cm^3 K mol^{-1} .

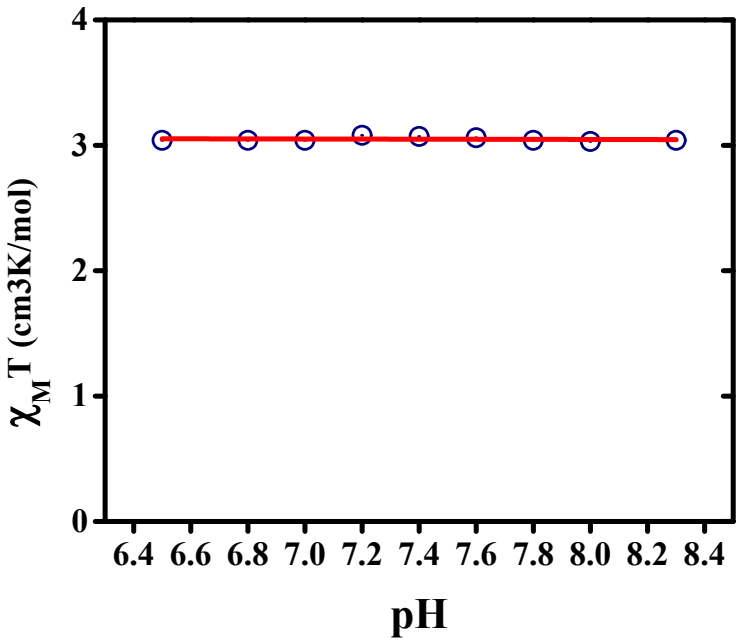

Fig. S24 Variable-pH magnetic susceptibility data for [Ni(**TPTA**)Cl]$^{+1}$ in aqueous solutions containing 20 mM HEPES and 100 mM NaCl at 37 °C, obtained using the Evans .Circles represent experimental data and the solid black line denotes the average value of $\chi_M T = 3.05 \pm 0.02$ cm^3 K mol^{-1} .

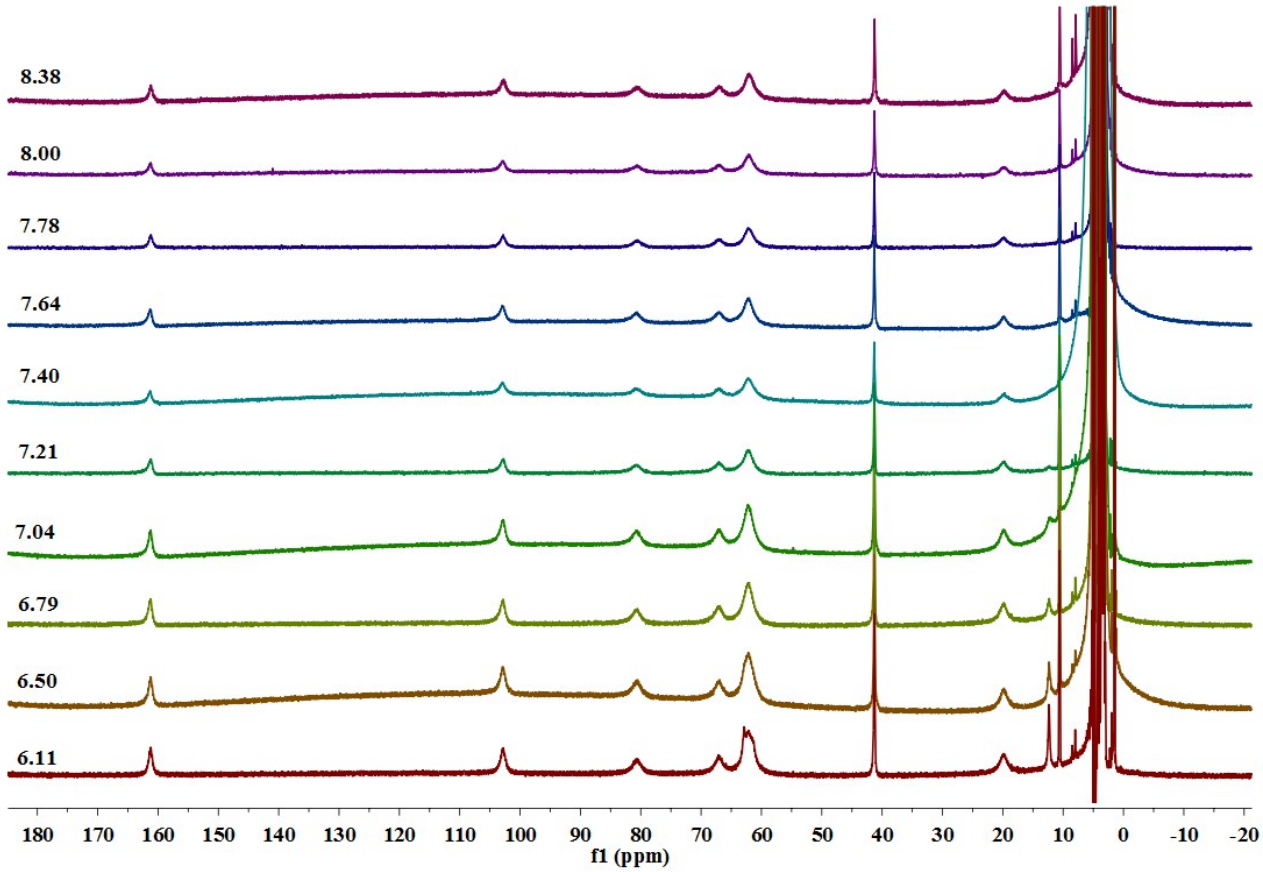

Fig. S25 Variable-pH ^{1}H NMR spectra of 10 mM of [Co(**TPTA**)]$^{+2}$ in aqueous solutions containing 20 mM HEPES and 100 mM NaCl buffered at various pH values at 37 °C.

^{1}H NMR of Dissociation study

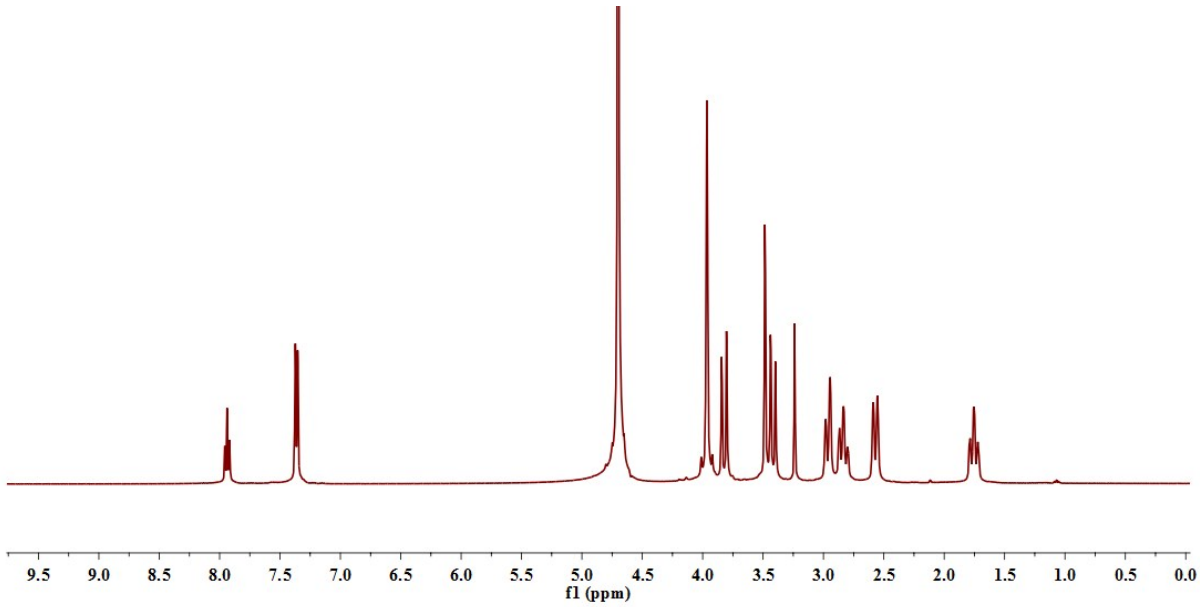

Fig. S26 ^{1}H NMR spectra of [Zn(**TPTA**)]$^{+2}$ complex in D_2O.

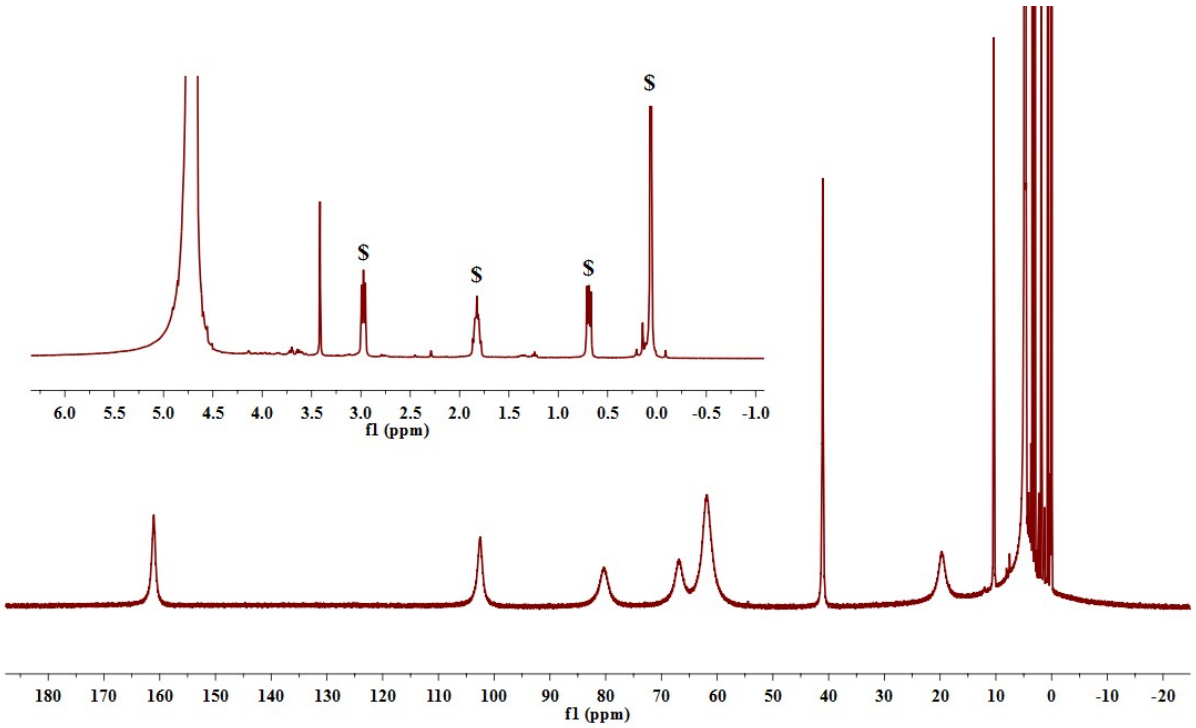

Fig. S27 ^{1}H NMR spectra of 10 mM [Co(**TPTA**)]$^{+2}$**,** 100 mM NaCl, 5 mM 3-(trimethylsilyl)-1-propanesulfonic acid sodium salt ($) at pD 7.0 as a standard solution for dissociation at 37 °C. Inset represents the diamagnetic region.

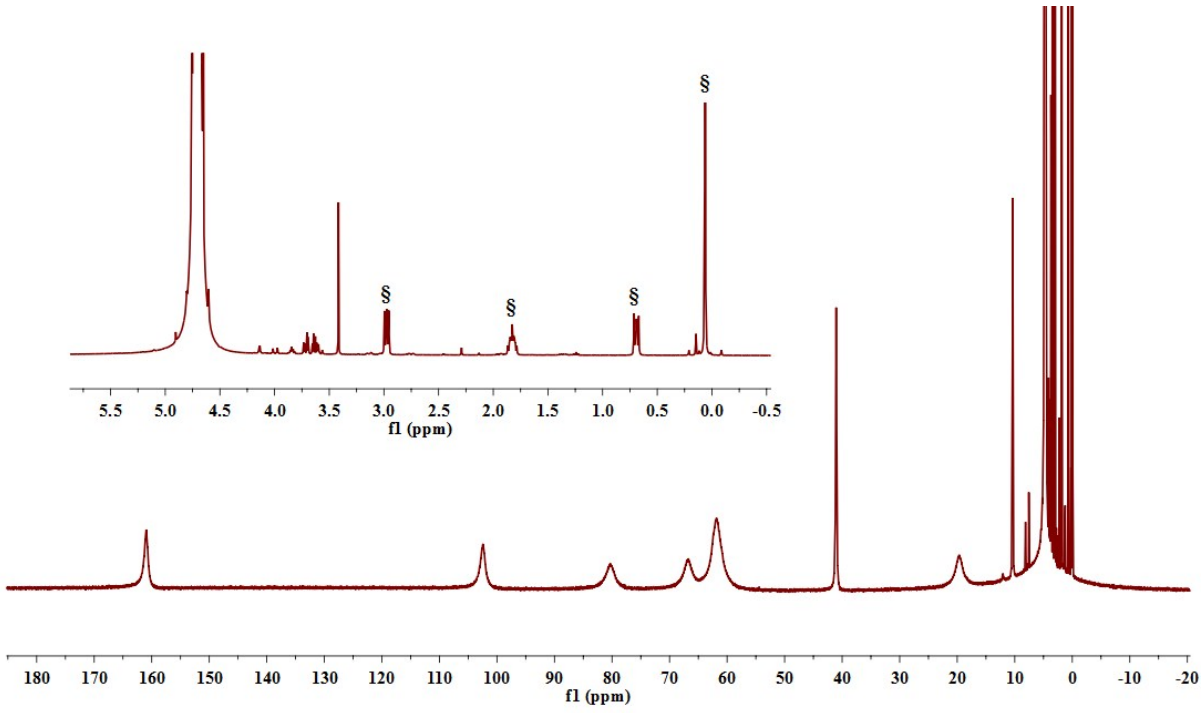

Fig. S28 ^{1}H NMR spectra of 12.5 mM [Co(**TPTA**)]$^{+2}$, 100 mM NaCl, 5 mM 3-(trimethylsilyl)-1-propanesulfonic acid sodium salt (§) at pD 3.96 after 72 hour of incubation at 37 °C. The

percentage of dissociation of [Co(**TPTA**)]$^{+2}$ was calculated by integrating paramagnetic peaks at 102 and 161 ppm verses standard. Inset represents the diamagnetic region. Peaks at 3.5 -4.0 ppm represent the newly formed free ligand in acidic solution.

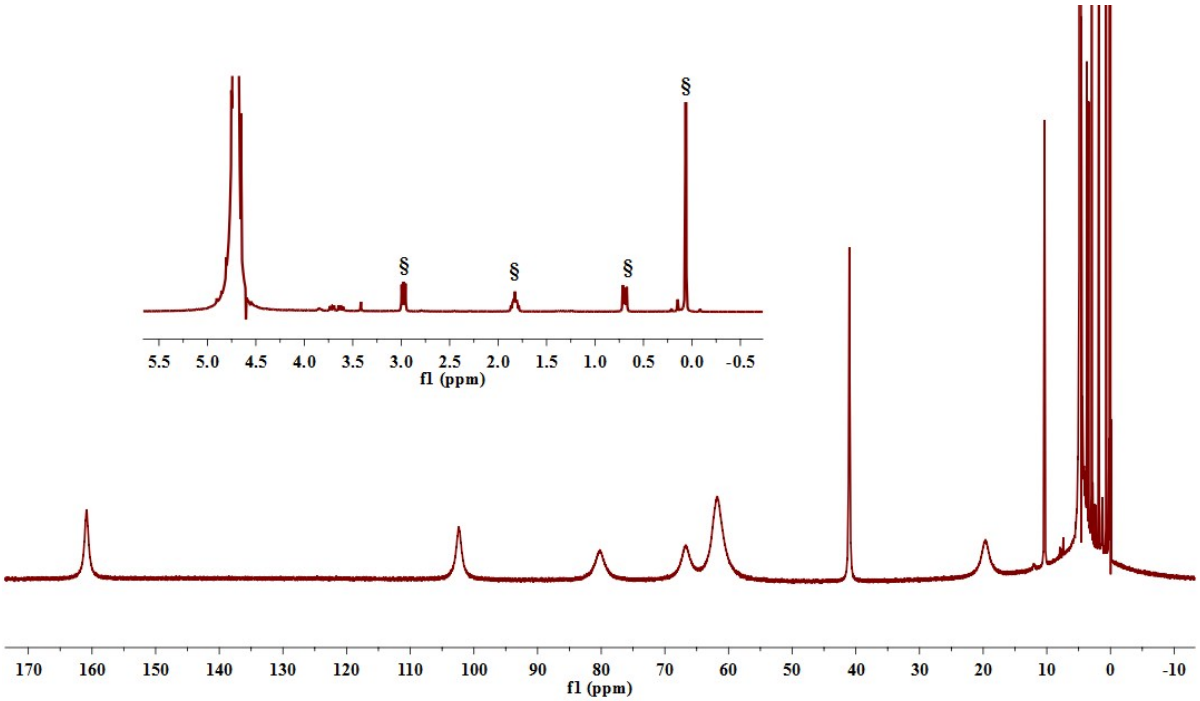

Fig. S29 ^{1}H NMR spectra of 10.5 mM [Co(**TPTA**)]$^{+2}$, 100 mM NaCl, 0.4 mM Na_2HPO_4, 25mM K_2CO_3 at pD 7.34 after 72 hour of incubation at 37 °C. The 3 mM 3-(trimethylsilyl)-1-propanesulfonic acid sodium salt (§) was added as a reference. The percentage of dissociation of [Co(**TPTA**)]$^{+2}$ was calculated by integrating paramagnetic peaks at 102 and 161 ppm verses standard. Inset represents the diamagnetic region.

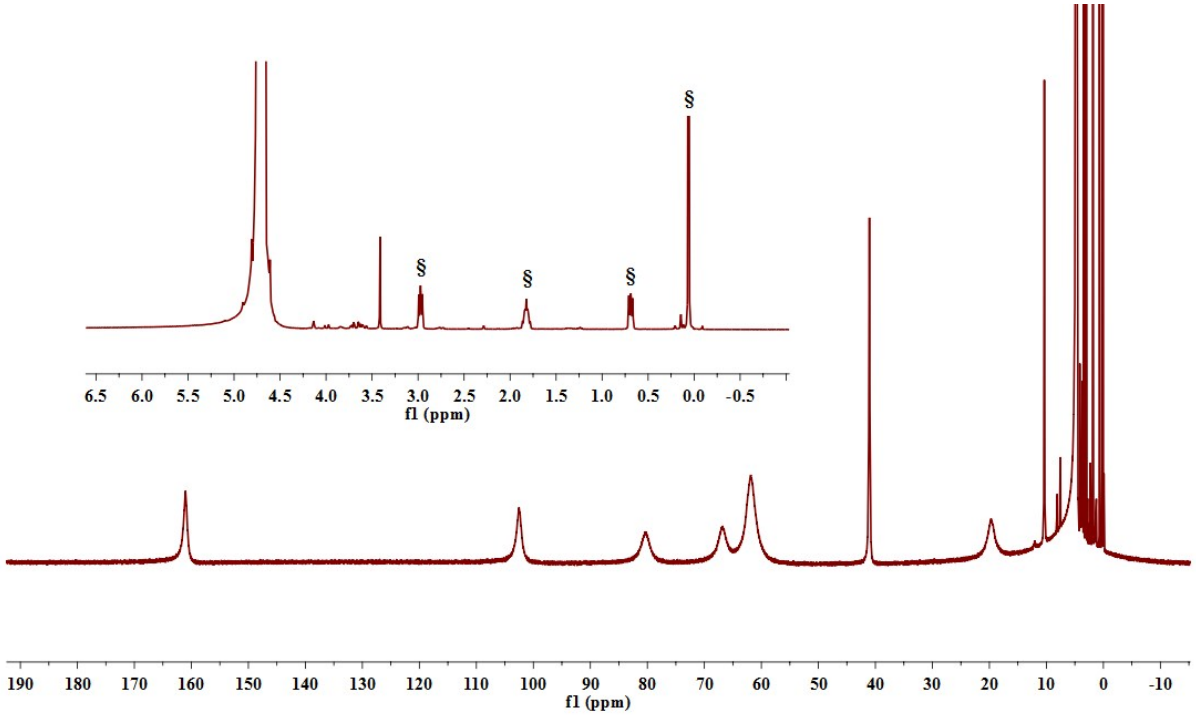

Fig. S30 ^{1}H NMR spectra of 10 mM [Co(**TPTA**)]$^{+2}$, 100 mM NaCl, 5 mM 3-(trimethylsilyl)-1-propanesulfonic acid sodium salt (§), incubated with 10 mM $ZnCl_2$ at pD 7.01 after 72 hours of incubation at 37 ºC. Spectrum showed no evidence of free ligands in the solution. Inset represents the diamagnetic region.

Determination of Exchange rate constant in buffered medium

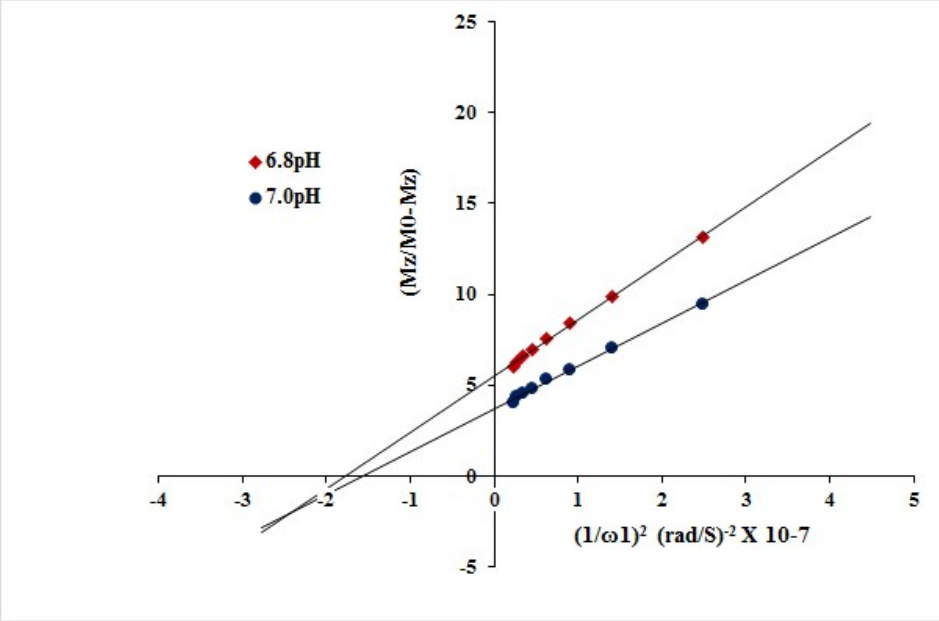

Fig. S31 Experimental data for exchange rate measurement of [Co(**TPTA**)]$^{+2}$ in buffered medium at pH 6.8 and 7.0. The desired linear relationship of $M_z/(M_0-M_z)$ as a function of $1/\omega_1^2$ (rad/sec)$^{-2}$ x 10^{-7} recorded at 9.4 T of 10 mM complex in 100 mM NaCl and 20 mM HEPES buffer. RF presaturation pulse was applied for 4 s with varying saturation power of 7.5 µT to 25 µT.

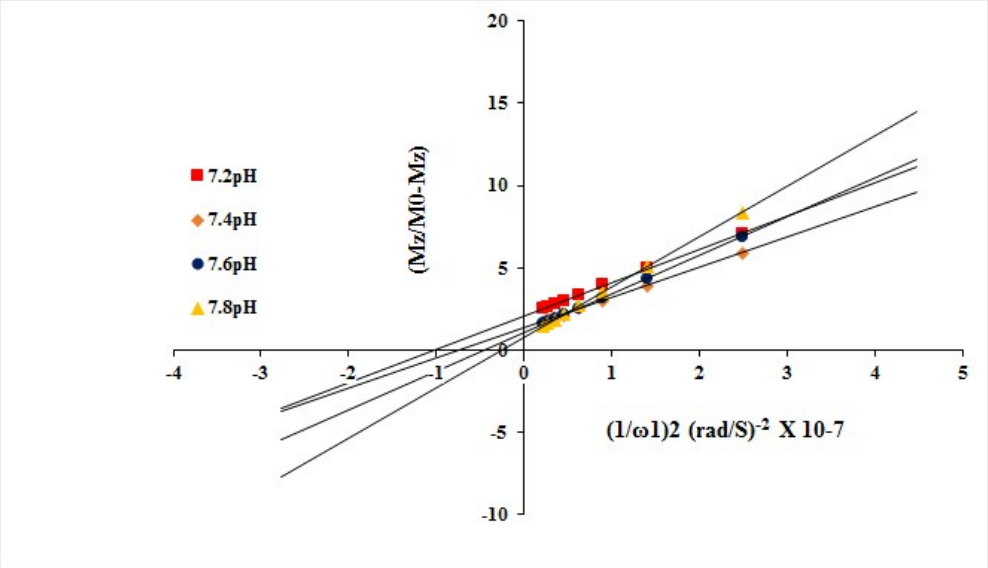

Fig. S32 Experimental data for exchange rate measurement of [Co(**TPTA**)]$^{+2}$ in buffered medium from pH 7.2-7.8. The desired linear relationship of $M_z/(M_0-M_z)$ as a function of $1/\omega_1^2$ $(rad/sec)^{-2}$ x 10^{-7} recorded at 9.4 T of 10 mM complex in 100 mM NaCl and 20 mM HEPES buffer. RF presaturation pulse was applied for 4 s with varying saturation power of 7.5 µT to 25 µT.

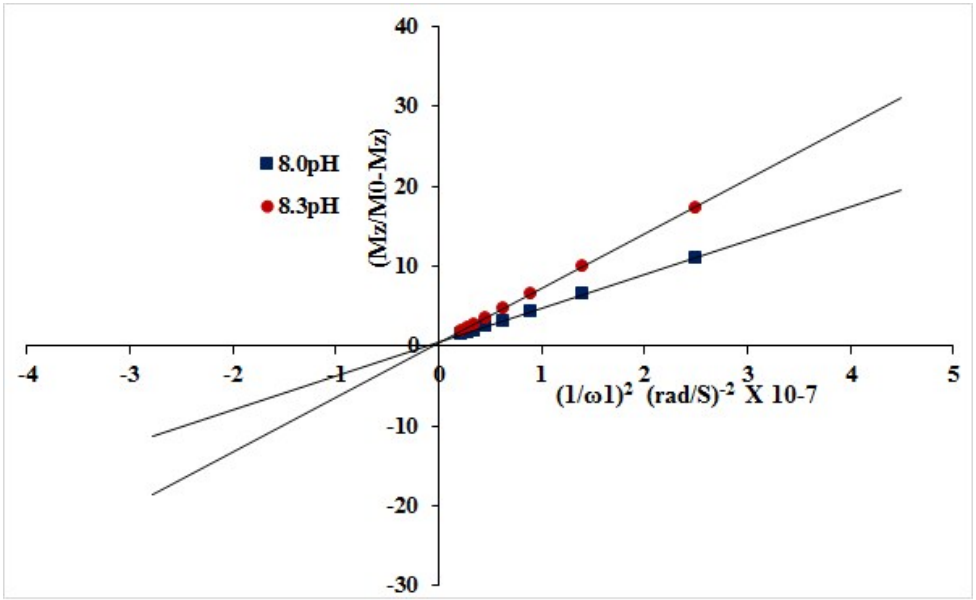

Fig. S33 Experimental data for exchange rate measurement of [Co(**TPTA**)]$^{+2}$ in buffered medium at pH 8 and 8.3. The desired linear relationship of $M_z/(M_0-M_z)$ as a function of $1/\omega_1^2$ $(rad/sec)^{-2}$ x 10^{-7} recorded at 9.4 T of 10 mM complex in 100 mM NaCl and 20 mM HEPES buffer. RF presaturation pulse was applied for 4 s with varying saturation power of 7.5 µT to 25 µT.

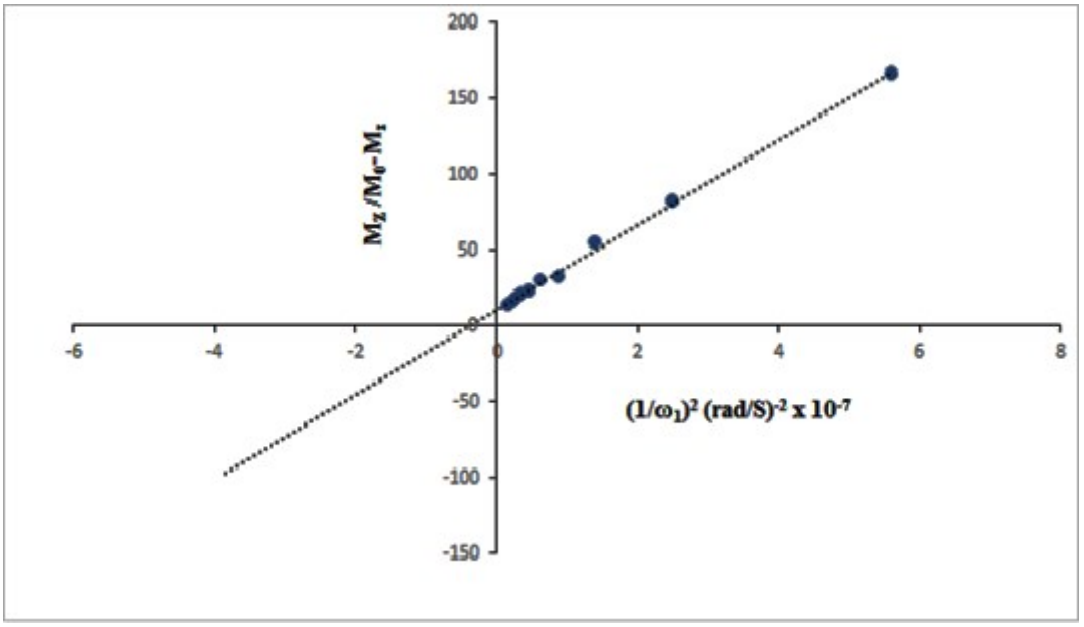

Fig. S34 Experimental data for exchange rate measurement of [Ni(**TPTA**)Cl]$^{+1}$ in buffered medium at 7.4.$M_z/(M_0-M_z)$ is plotted as a function of $1/\omega_1^2$ $(rad/sec)^{-2}$ x 10^{-7} . The exchange constant measurement experiments were recorded at 9.4 T for 40 mM complex in 100 mM NaCl and 20 mM HEPES buffer. RF presaturation pulse was applied for 4 s with varying saturation power from 5 μT to 30 μT.

Determination of Exchange rate constant in different media

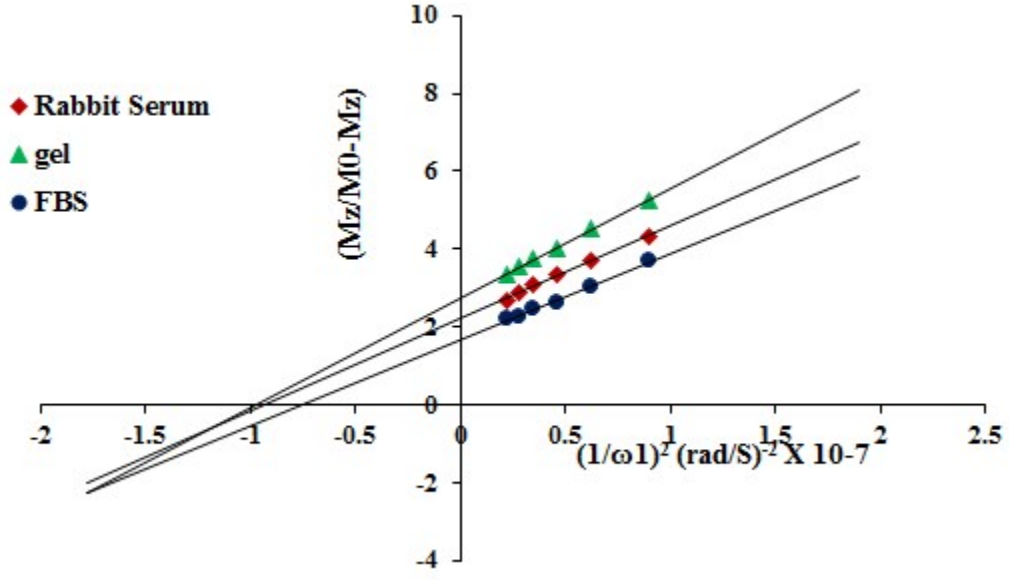

Fig. S35 Experimental data for exchange rate measurement of [Co(**TPTA**)]$^{+2}$ in biological media. The desired linear relationship of $M_z/(M_0-M_z)$ as a function of $1/\omega_1^2$ $(rad/sec)^{-2}$ x 10^{-7} recorded at 9.4 T of 10 mM complex in 100 mM NaCl, 20 mM HEPES and 4% Agarose gel

(red squares), in rabbit serum (brown circle) and in FBS (blue diamond) at pH 7.4. RF presaturation pulse was applied for 2 s with varying saturation power of 12 μT to 25 μT.

Table S1 Proton exchange rate constants for [Co(**TPTA**)]$^{+2}$ at different pH of 10 mM complex in 100 mM NaCl and 20 mM HEPES.

pH of the [Co(**TPTA**)]$^{+2}$ complex in buffer	6.8	7.0	7.2	7.4	7.6	7.8	8.0	8.3
Exchange rate constant (s^{-1})	2379	2519	3047	3691	4626	6280	9134	13380

Concentration dependence of CEST effect

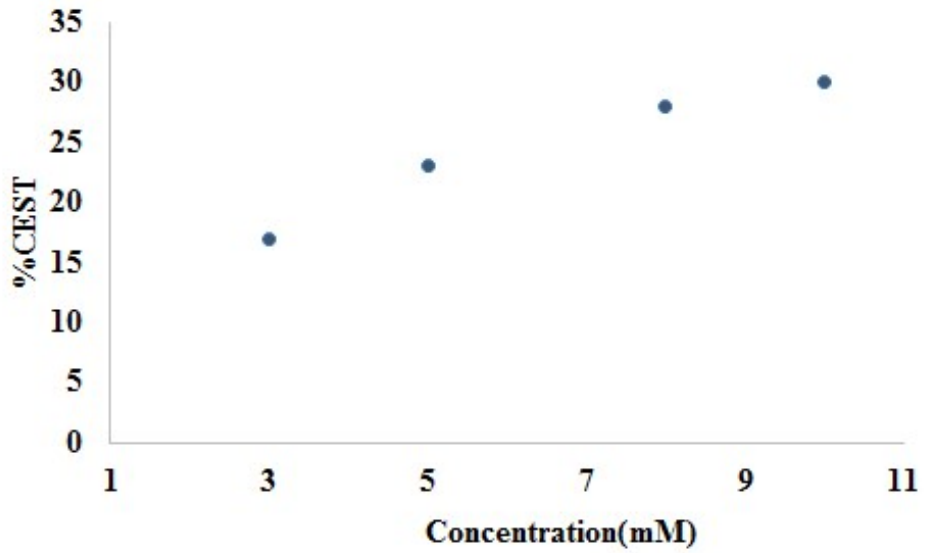

Fig. S36 Concentration dependent study of CEST effect at physiological condition (pH 7.4, 37 °C). CEST effects measured for 3 mM, 5 mM, 8 mM and 10 mM [Co(**TPTA**)]$^{+2}$ complex in 100 mM NaCl and 20 mM HEPES buffer. RF presaturation pulse was applied for 2 s with B_1=25μT.

Dissociation study

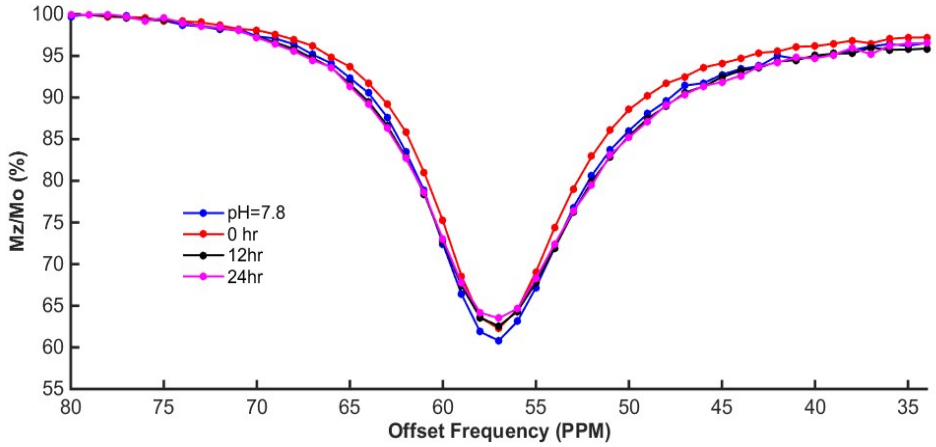

Fig. S37 Time lapsed CEST effect study at physiological condition (pH 7.8, 37 °C). CEST effect was measured for 10 mM [Co(**TPTA**)]$^{+2}$ complex in 100 mM NaCl and 20mM HEPES buffer without 25 mM K_2CO_3, 0.40 mM Na_2HPO_4 and with the addition of 25 mM K_2CO_3, 0.40 mM Na_2HPO_4 immediately after preparing the solution (0 hour), after half a day (12 h) and after a complete day (24 h). No significant dissociation was observed in one day.

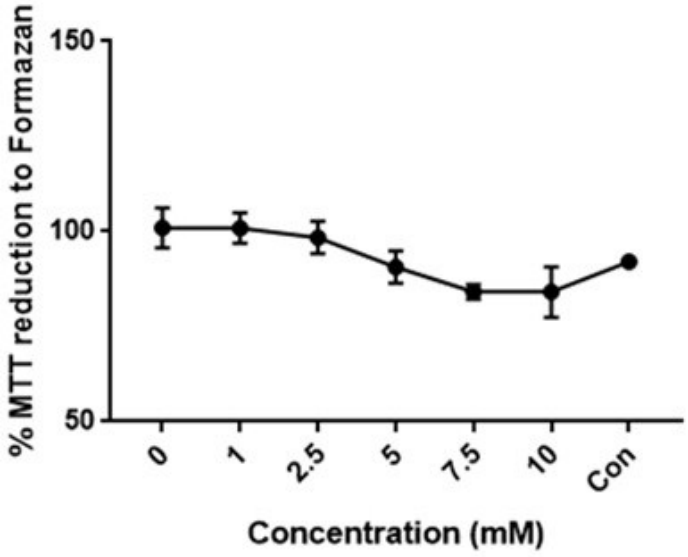

Fig. S38 Cell-viability studies using the MTT assay of different concentration of [Co(**TPTA**)]$^{+2}$ complex [Co(**TPTA**)]$^{+2}$ on HEK cell after incubation for 24 h at 37 ºC.

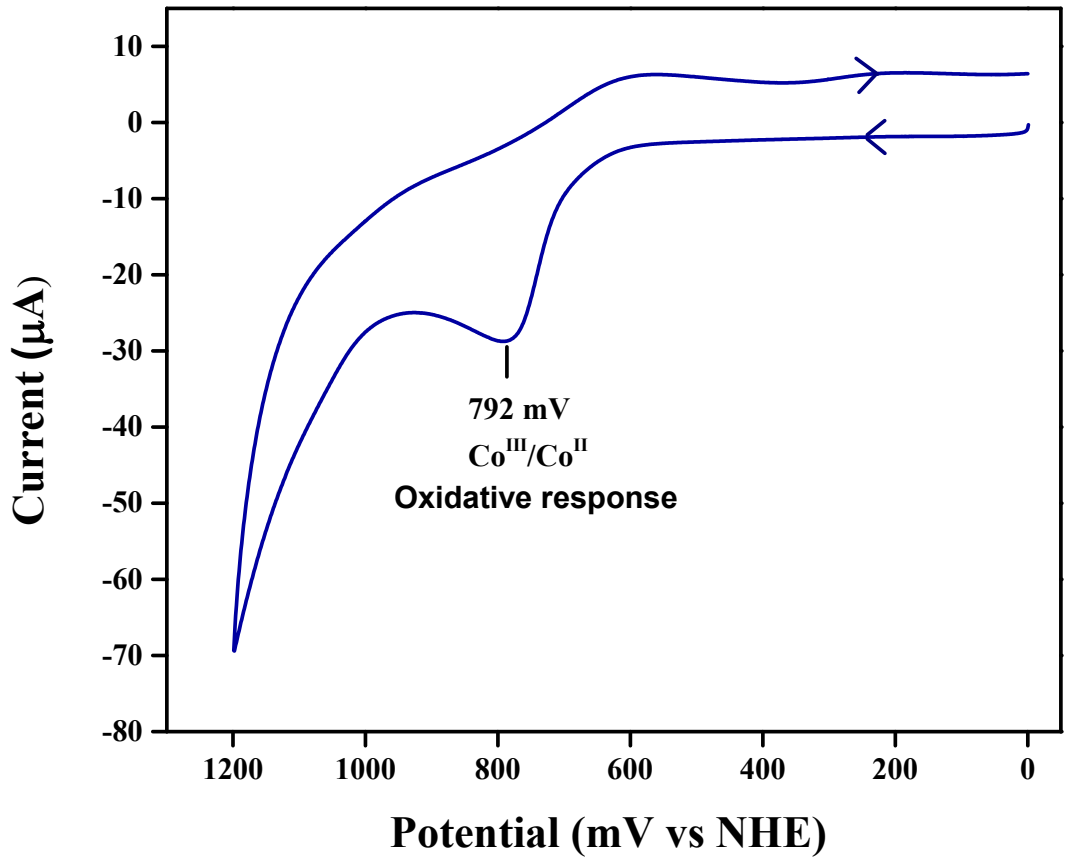

Fig. S39 Cyclic voltammogram for 1 mM of [Co(**TPTA**)]$^{+2}$ in an aqueous solution containing 20 mM HEPES and 100 mM NaCl buffered at pH 7.4. Measurements was carried out at ambient temperature using a glassy carbon electrode as a working electrode with a 100 mV/s scan rate. The potential given were converted to the normal hydrogen electrode (NHE).

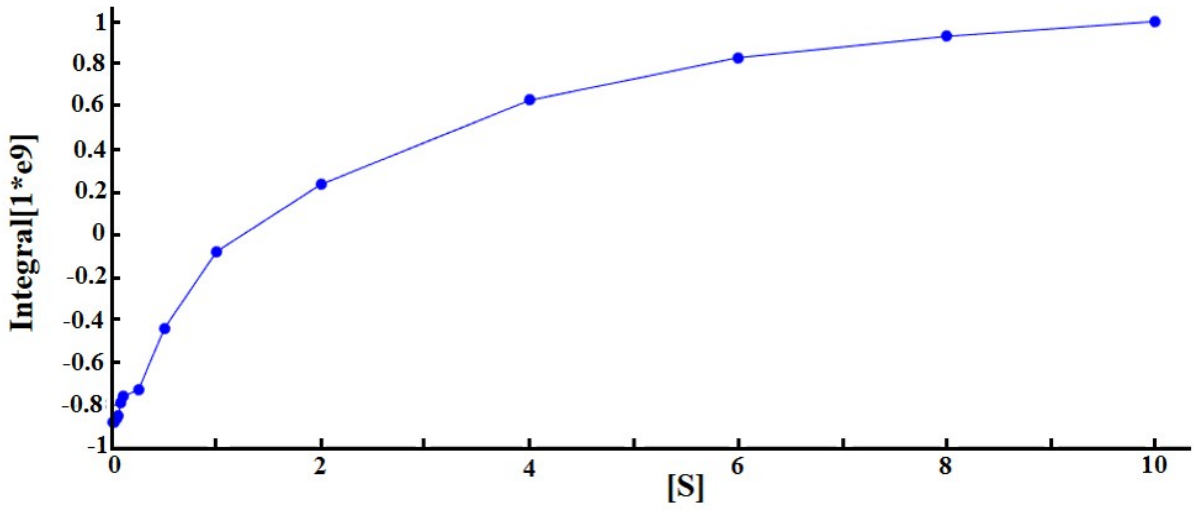

Fig. S40 T_1 relaxation plot of water in 20 mM HEPES and 100 mM NaCl buffered at pH 7.4 in absence of $(Co[TPTA])^{2+}$.Fitting was done using topspin 2.1. The longitudinal relaxation time constants for water proton is found to be 1.83 s

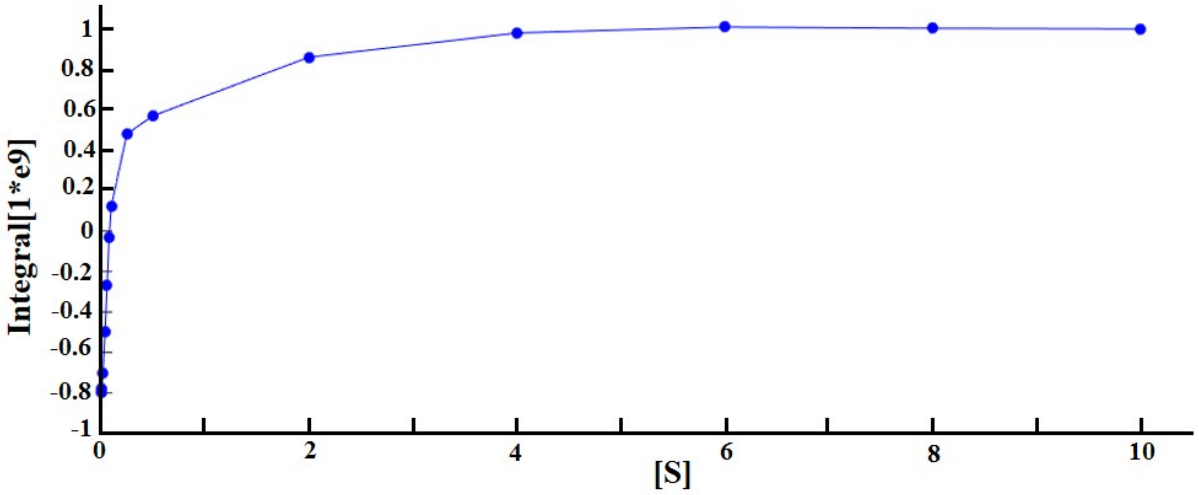

Fig. S41 T_1 relaxation plot of water in 20 mM HEPES and 100 mM NaCl buffered in the presence of $(Co[TPTA])^{2+}$ at pH 7.4. Fitting was done using topspin 2.1. The longitudinal relaxation time constants for water proton is found to be 0.14 s

Relaxivity calculation:

Relaxivity (R)= $\frac{1}{c}\left(\frac{1}{T_1^{'}}-\frac{1}{T_1}\right)$ where $T_1^{'}$ and T_1 are the longitudinal relaxation time constants of water protons in the presence and in absence of $(Co[TPTA])^{2+}$ respectively.

$$R=\frac{1}{10}(7.14-0.55)=0.66 \quad (mM)^{-1}s^{-1}$$

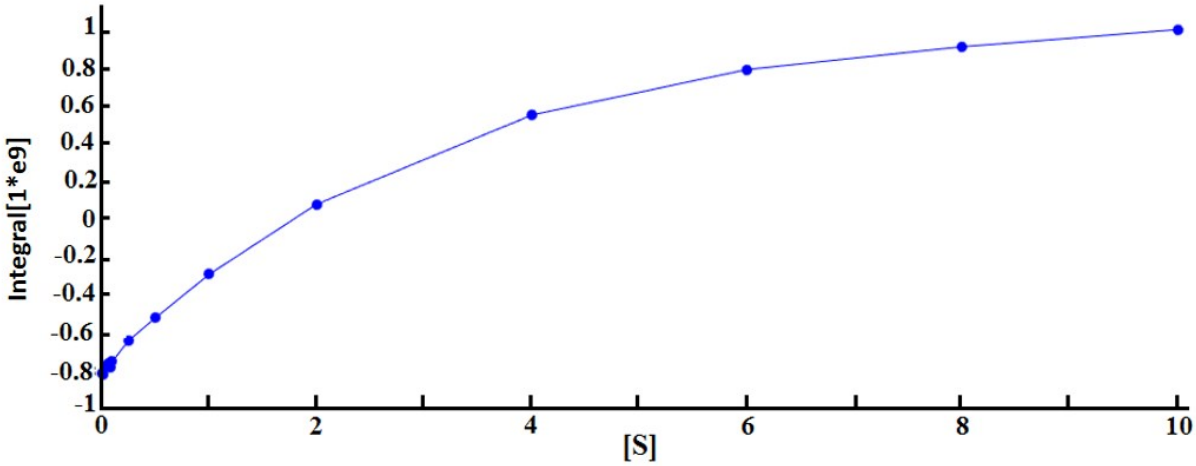

Fig. S42 T_1 relaxation plot of water in 4% Agarose gel at pH 7.4 in absence of $(Co[TPTA])^{2+}$.Fitting was done using topspin 2.1. The longitudinal relaxation time constants for water proton is found to be 3.039s.

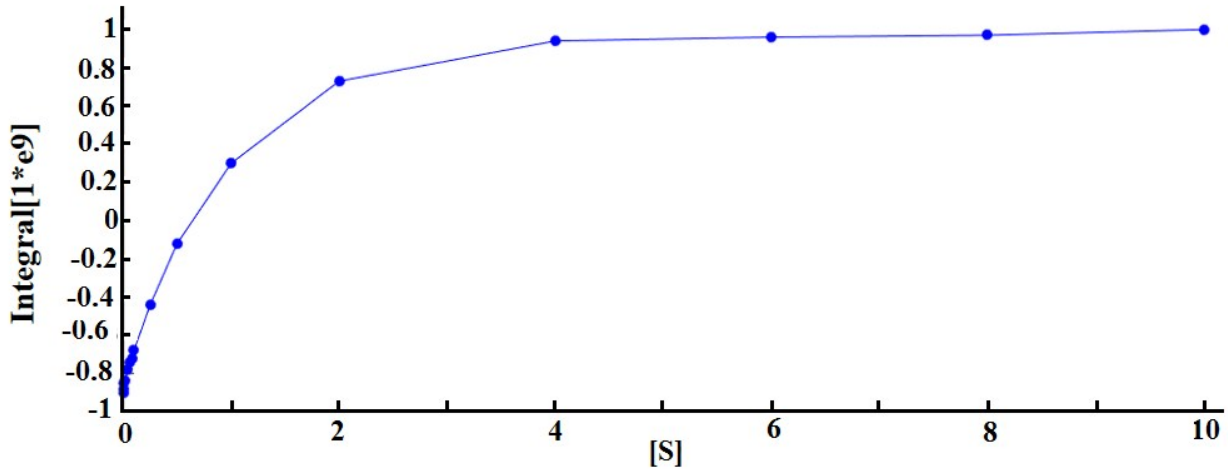

Fig. S43 T_1 relaxation plot of water in 4% Agarose gel in presence of $(Co[TPTA])^{2+}$ at pH 7.4. The fitting was done using topspin 2.1. The longitudinal relaxation time constants of water proton is found to be 1.06s.

Relaxivity calculation:

Relaxivity (R)= $\frac{1}{c}\left(\frac{1}{T_1'}-\frac{1}{T_1}\right)$ where T_1' and T_1 are the longitudinal relaxation time constants of water protons in the presence and in absence of $(Co[TPTA])^{2+}$ respectively.

R= $\frac{1}{10}(0.94-0.33) = 0.06\ (mM)^{-1}s^{-1}$

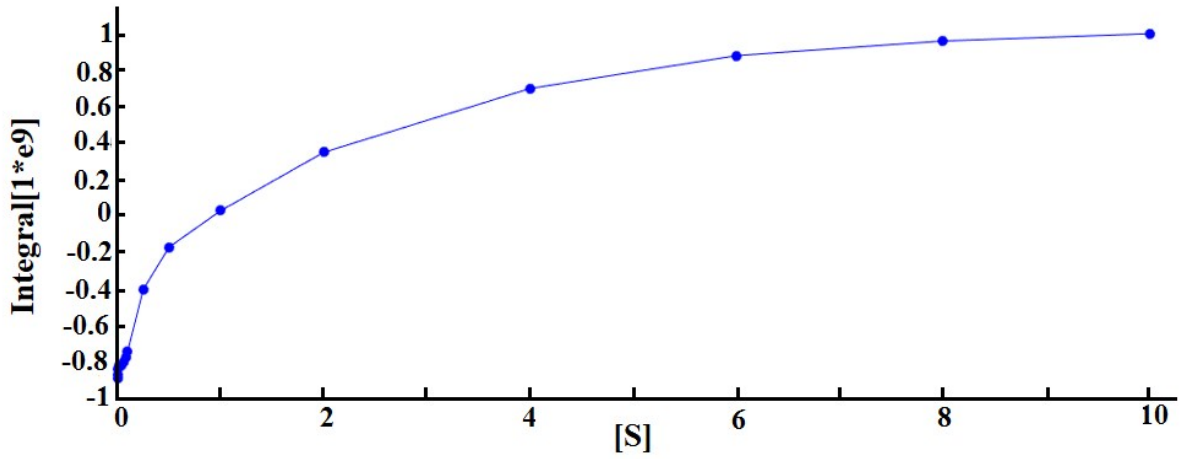

Fig. S44 T_1 relaxation plot of water Rabbit Serum at pH 7.4 in the absence of $(Co[TPTA])^{2+}$.Fitting was done using topspin 2.1. The longitudinal relaxation time constants for water proton is found to be 1.469s.

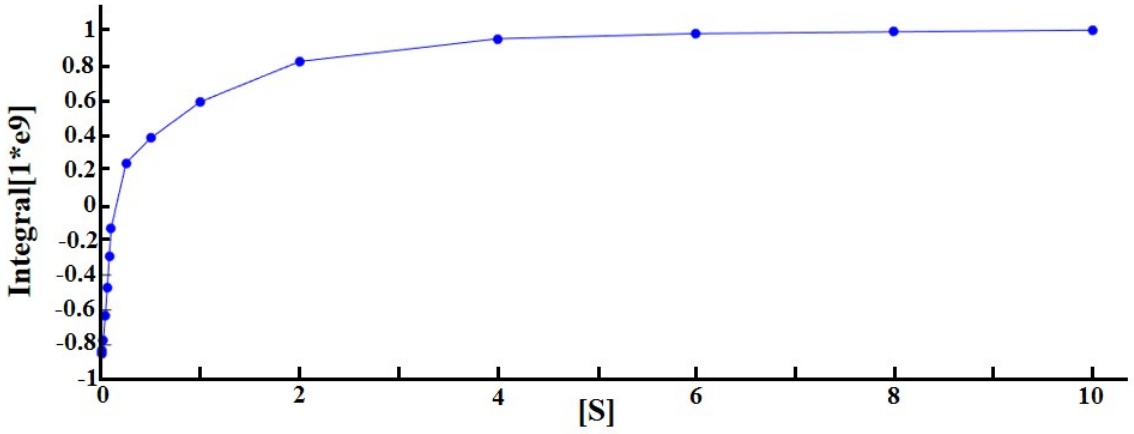

Fig. S45 T1 relaxation plot of water Rabbit serum in the presence of $(Co[TPTA])^{2+}$ at pH 7.4. The fitting was done using topspin 2.1. The longitudinal relaxation time constants for water proton is found to be 0.289s.

Relaxivity calculation:

Relaxivity (R)= $\frac{1}{c}\left(\frac{1}{T_1^{'}}-\frac{1}{T_1}\right)$ where $T_1^{'}$ and T_1 are the longitudinal relaxation time constants of water protons in the presence and in absence of $(Co[TPTA])^{2+}$ respectively.

R= $\frac{1}{10}(3.46-0.68)$ = 0.28 $(mM)^{-1}s^{-1}$

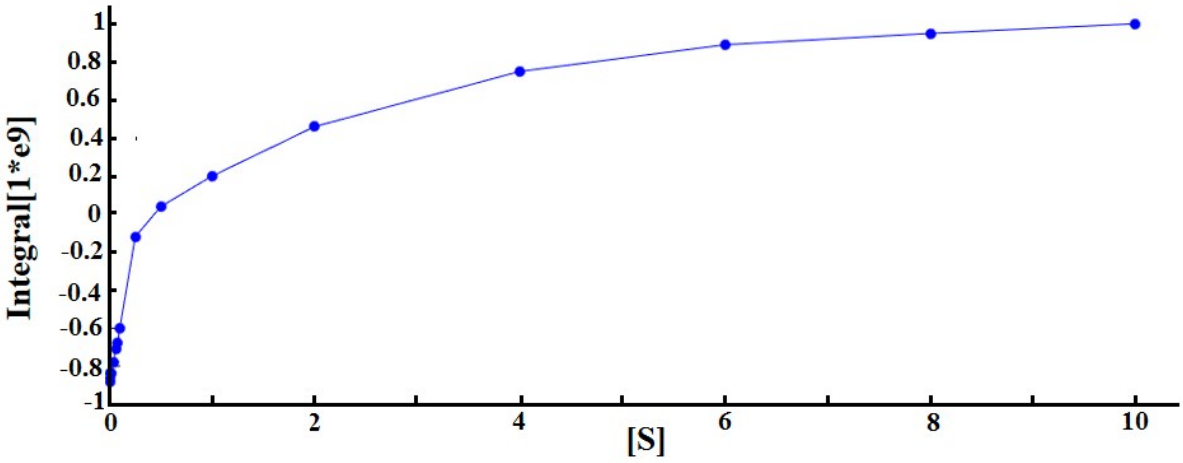

Fig. S46 T1 relaxation plot of water in FBS at pH 7.4 in the absence of $(Co[TPTA])^{2+}$. The fitting was done using topspin 2.1. The longitudinal relaxation time constants for water proton is found to be 0.894s.

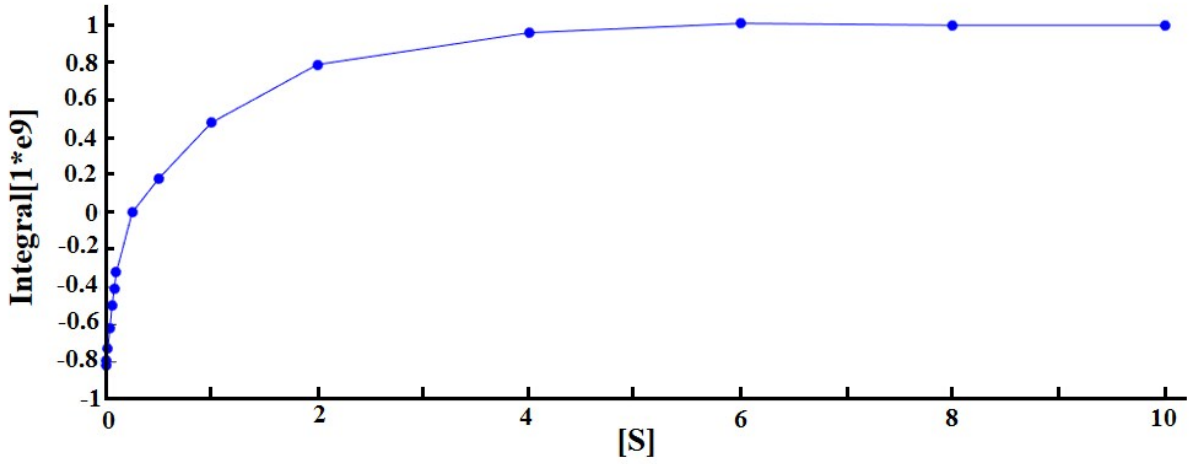

Fig. S47 T1 relaxation plot of water in FBS in the presence of $(Co[TPTA])^{2+}$ at pH 7.4. The fitting was done using topspin 2.1. The longitudinal relaxation time constants for water proton is found to be 0.595s.

Relaxivity calculation:

Relaxivity (R)= $\frac{1}{c}\left(\frac{1}{T_1^{'}}-\frac{1}{T_1}\right)$ where $T_1^{'}$ and T_1 are the longitudinal relaxation time constants of water protons in the presence and in absence of $(Co[TPTA])^{2+}$ respectively.

R= $\frac{1}{10}(1.68-1.14)$ =0.05 $(mM)^{-1}s^{-1}$

Table S2 Selected Bond Length (Å) and Bond Angles (deg) for [Co(**TPTA**)]·Cl_2·$2H_2O$ and [Ni(**TPTA**)Cl]$_2$·Cl_2·$0.5H_2O$.

[Co(**TPTA**)]·**Cl_2·$2H_2O$**		[Ni(**TPTA**)Cl]$_2$·**Cl_2·$0.5H_2O$**	
Bond Length			
Co(1)-N(1)	2.127(6)	Ni(1)-N(1)	2.015(3)
Co(1)-N(2)	2.256(6)	Ni(1)-N(2)	2.220(3)
Co(1)-N(4)	2.199(6)	Ni(1)-N(4)	2.123(3)
Co(1)-N(6)	2.327(6)	Ni(1)-N(6)	2.232(3)
Co(1)-O(1)	2.231(5)	Ni(1)-O(1)	2.083(3)
Co(1)-O(2)	2.171(5)	Ni(1)-Cl(1)	2.3367(9)
Co(1)-O(3)	2.154(5)		
Bond Angles			
N(1)-Co(1)-O(3)	104.5(2)	N(1)-Ni(1)-O(1)	171.74(11)
N(1)-Co(1)-O(2)	172.9(2)	N(1)-Ni(1)-N(4)	91.96(12)
O(3)-Co(1)-O(2)	82.3(2)	O(1)-Ni(1)-N(4)	80.51(11)

N(1)-Co(1)-N(4)	102.0(2)	N(1)-Ni(1)-N(2)	80.40(12)
O(3)-Co(1)-N(4)	129.6(2)	O(1)-Ni(1)-N(2)	95.30(12)
O(2)-Co(1)-N(4)	74.6(2)	N(4)-Ni(1)-N(2)	83.72(11)
N(1)-Co(1)-O(1)	101.5(2)	N(1)-Ni(1)-N(6)	78.84(11)
O(3)-Co(1)-O(1)	78.26(18)	O(1)-Ni(1)-N(6)	103.42(11)
O(2)-Co(1)-O(1)	77.55(17)	N(4)-Ni(1)-N(6)	83.16(10)
N(4)-Co(1)-O(1)	136.0(2)	N(2)-Ni(1)-N(6)	154.96(11)
N(1)-Co(1)-N(2)	74.4(2)	N(1)-Ni(1)-Cl(1)	95.05(9)
O(3)-Co(1)-N(2)	149.2(2)	O(1)-Ni(1)-Cl(1)	92.48(8)
O(2)-Co(1)-N(2)	98.7(2)	N(4)-Ni(1)-Cl(1)	172.98(8)
N(4)-Co(1)-N(2)	79.4(2)	N(2)-Ni(1)-Cl(1)	97.20(8)
O(1)-Co(1)-N(2)	72.0(2)	N(6)-Ni(1)-Cl(1)	98.42(8)
N(1)-Co(1)-N(6)	73.4(3)		
O(3)-Co(1)-N(6)	71.8(2)		
O(2)-Co(1)-N(6)	111.3(2)		
N(4)-Co(1)-N(6)	76.0(2)		
O(1)-Co(1)-N(6)	146.9(2)		
N(2)-Co(1)-N(6)	133.8(2)		